GEORG-AUGUST-UNIVERSITÄT
GÖTTINGEN

Fakultät für
Physik

Bachelor Thesis

Dynamical phase transitions of wet granular matter

Dynamische Phasenübergänge von feuchter granularer Materie

prepared by

Stefanie Strauch

from Berlin

at the Max Planck Institute for Dynamics and Self-Organization

Thesis period: 10th January 2011 until 18th April 2011

First referee: Prof. Dr. Stephan Herminghaus

Second referee: Prof. Dr. Annette Zippelius

Abstract

The dependence of the dynamical behavior of wet granular matter on the amount of liquid was studied experimentally. By vibrating a sample of small glass beads mixed with silicon oil vertically, three phase transitions were observed. Particularly prominent was a fluid-gas coexistence, whose onset seemed to be solely energy dependent. Phase diagrams obtained at different liquid contents are presented and compared with each other. It was found that the energy which is dissipated when a liquid bridge ruptures determines the onset of the fluid-gas coexistence over a wide range of liquid contents, although the morphology of the liquid distribution changes drastically.

Contents

1. Introduction

Probably the most well-known example of a wet granular material is a sandcastle. While a handful of dry sand simply trickles through one's fingers, wet sand is a much more pasty material. The sand grains are held together by liquid bridges which form at the contact areas between neighboring grains. Once a liquid bridge is formed, it exerts an attractive force, the capillary force, on the grains. Thus, a sample of wet sand has an enhanced mechanical stability compared to a dry one. This allows one to build an arbitrarily shaped sandcastle, which is able to withstand the force of gravity and retain its shape. The capillary force has been studied experimentally as well as theoretically (see for example [5, 10, 19]), whereas the sand grains usually have been replaced by small, round glass beads. Furthermore, Scheel et al. [15] studied the dependence of the mechanical stability of a pile of wet glass beads on the amount of added liquid. On the one hand, a certain minimum amount of liquid in the sample is required [10]. Otherwise, the surface roughness of the beads causes the liquid to fill the small crevices of the glass surface and prevent it from accumulating at the contact areas to form liquid bridges. On the other hand, if too much liquid is present in the sample, the cohesive effect of the liquid diminishes and the mechanical strength of the sample is weakened. This becomes quite clear when picturing the sandcastle at the beach again: It is impossible to build a sandcastle out of a sand pile containing too much water, because it behaves just as a liquid. However, within the range in-between the mechanical stability of wet granular matter does not depend on the amount of liquid.

What is more, the dynamics of the formation and rupture of a liquid bridge leads to different phase transitions of wet granular matter ([8, 11]). Since two approaching particles are not connected by a liquid bridge, they do not experience a force. Once they come into contact though, the newly formed liquid bridge exerts an attractive force on the particles. This force persists during the movement of the particles away from each other, at least until a critical distance is reached. At this point, the bridge ruptures and the liquid distributes itself back onto the surface of the particles. It is this hysteretic nature of the capillary force that gives rise to a well-defined amount of energy which is dissipated each time a liquid bridge breaks. If energy is injected into a sample of wet granular material, it can be transformed into different phases, depending on the balance between injected and dissipated energy. Referring to the notation of systems in thermal equilibrium, the wet granulate can reside in a

solid, liquid or gaseous phase [7]. Huang et al. [11] applied a vertical agitation to a pile of glass beads mixed with water and thereby observed those three phases. In addition, a fluid-gas coexistence was observed. While the phase transition from the solid to the fluid phase is independent of the injected energy, the onset of the fluid-gas coexistence is independent of the force. Furthermore, the onset seems to be solely determined by the amount of energy which is dissipated when a liquid bridge ruptures.

In this thesis, it was investigated experimentally how increasing the amount of liquid in the system affects the dynamical phase transitions of wet granular matter. The question raised was whether its dynamical behavior is insensitive to the amount of liquid, as is the case with its mechanical strength, or whether additional effects come into play. The experimental approach was similar to that of Huang et al. [11]: The energy was injected into a sample of glass beads mixed with silicon oil by a vertical agitation. Each phase transition was depicted in a phase diagram and compared with earlier results from Huang et al. [11] and Röller [14]. Finally, the possible influence of a varying amount of liquid on the phase transitions was investigated by comparing the different phase diagrams with each other.

2. Wet granular matter

In general, granular matter consists of macroscopic particles which interact only once they actually touch. The inelasticity of these collisions manifests itself in the transfer of a fraction of kinetic energy of the particles prior to the collision to internal atomic degrees of freedom. Hence the relative momentum $p = |p_1 - p_2|$ of two particles is decreased after contact. The restitution coefficient $\epsilon := p_f/p_i$ is introduced as a measure of the inelasticity of such a collision, whereas the indices f and i correspond to the final and initial relative momentum, respectively. Since other forces like Van der Waals or gravitational forces can be neglected, the dominant force present in the system is a purely repulsive one. Furthermore, if one defines the temperature of a granular gas to be proportional to the average kinetic energy of a particle (in analogy to the kinetic gas theory), one finds that the temperatures are in the Terakelvin range. A typical velocity in this research ranges from 1 cm/s to 50 cm/s and the average mass of a single particle is approximately 21 orders of magnitude larger in comparison to an atom. In fact, this huge mass difference is responsible for the large granular temperatures. Coupling this heat bath via interparticle collisions to the atomic degrees of freedom of said particles leads to a non-equilibrium situation, since the atomic degrees of freedom are at room temperature. The inelastic collisions therefore account for a non-equilibrium, which is the dominant factor of the behavior of dry granular matter.

Adding a wetting liquid to the particles, capillary forces are being introduced to the system. The surface tension of the liquid causes the formation of a so-called capillary bridge once two particles touch. Various calculations of these capillary forces have been conducted before (see for example [5, 19]), whereas the result depends on, amongst others, the separation distance of the particles, the size of the particles, the volume, and geometry of the liquid bridge. In order to derive an analytical expression, approximations are inevitable. In the following, the particles are assumed to be perfectly smooth spheres of equal size. The roughness of the glass beads under research in this thesis can be safely neglected. For very small liquid contents, only a few capillary bridges are formed, since the liquid fills the crevices of the uneven grain surface up first. Here, however, it is dealt with liquid contents that are beyond this regime, which ends at a liquid content of typically 10^{-3} [10].

In this thesis, the liquid content W is defined as the ratio of the volume of the liquid and the volume of the whole sample, and is thus a dimensionless quantity. In addition, the capillary bridge is approximated by a toroid. The surface tension γ can be pictured as the amount of energy which is needed in order to increase the surface area of a liquid. The resulting force $F_{s.t.}$ acting on the surface of that liquid is proportional to γ. The curvature of the liquid bridge gives rise to a hydrostatic pressure difference Δp between the interior of the bridge and its surroundings. Hence, a second force $F_{Laplace}$, which is proportional to Δp and the cross-sectional area of the bridge, is generated. Additional forces like the buoyancy force are negligibly small [19], and will not be considered. The pressure difference at a given point of the surface can be obtained from the Young-Laplace equation:

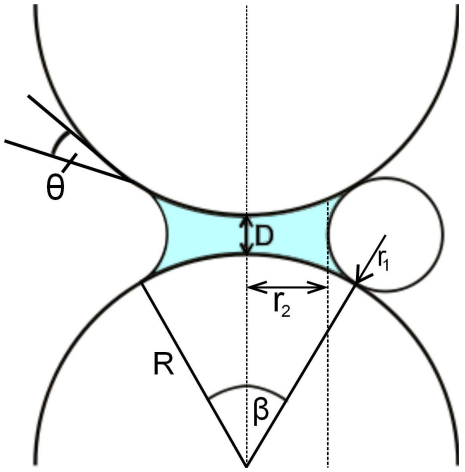

Figure 1: Two identical spheres with radius R are indicated. A capillary bridge is shown in the toroidal approximation.

$$\Delta p = \gamma \cdot \left(\frac{1}{r_1} + \frac{1}{r_2} \right), \tag{2.1}$$

where r_1 and r_2 are the two radii of curvature which describe the curvature of the surface. In literature, the pressure difference is often termed Laplace pressure. Fig. 1 shows an example of a capillary bridge with a toroidal shape. Note that the pressure difference is negative, because r_1 is counted negative. Assuming $r_1 \ll r_2$, one gets $\Delta p \approx -\gamma / r_1$. All in all, the total capillary force F_{cap} is the sum of $F_{s.t.}$ and $F_{Laplace}$. If one further assumes the separation distance D between the spheres to be much smaller than r_2, $F_{Laplace}$ will dominate the total force which is then given by [5]:

$$F_{cap} \approx \frac{\gamma}{r_1} \pi R^2 \sin^2(\beta). \tag{2.2}$$

In the above formula R denotes the radius of the spheres and β is the half-filling bridge angle (fig. 1). In addition, Willett et al. [19] presented a polynomial fit for the total capillary force (including $F_{s.t.}$):

$$F_{cap} \approx \frac{2\pi R\gamma\cos(\theta)}{1 + 1.05 \cdot \sqrt{\frac{R}{V}}D + 2.5 \cdot \frac{R}{V}D^2}, \tag{2.3}$$

where V is the volume of a liquid bridge, θ the contact angle between the liquid-gas interface and a sphere, and D the distance between the two spheres. This fit is in good agreement with experimental data [19].

Another important quantity is the rupture distance D_{crit}, i.e., the length of the liquid bridge right before it ruptures. Again Willett et al. [19] provided an approximation of the best-fit equation for equal spheres:

$$D^*_{crit} = \left(1 + \frac{\theta}{2}\right) \cdot \left(V^{*1/3} + \frac{V^{*2/3}}{10}\right). \tag{2.4}$$

The star denotes the dimensionless quantities: $D^* = D/R$ and $V^* = V/R^3$.

The essential element determining the dynamics of wet granular matter is the hysteretic nature of the capillary force: When two particles approach each other, they do not experience a force. After having been in contact, the capillary bridge exerts an attractive force on the particles while they move apart. This force vanishes as soon as the separation D between the particles becomes larger than the critical distance D_{crit}, at which the bridge collapses. During this process a well defined amount of energy is being dissipated:

$$\Delta E_{cap} = \int_0^{D_{crit}} \mathrm{d}s\, F_{cap} = \alpha \cdot \gamma R^2 \cos(\theta). \tag{2.5}$$

The liquid content W is defined as the volume of liquid divided by the volume of the whole sample. In this thesis, water and silicon oil are used, and both wet the particles almost completely. Therefore the contact angle is nearly zero and $\cos(\theta) \approx 1$. The proportionality constant α is determined by Herminghaus [10]:

$$\alpha \approx 5.5\sqrt{V^*} \approx 15.92 \cdot \sqrt{\frac{W}{\rho N}}, \tag{2.6}$$

where ρ is the packing density, and N the average number of liquid bridges per sphere. It is straightforward to calculate the dimensionless volume V^* of one liquid bridge. If n is the number of identical particles with radius R in a container with volume V_{tot}, the packing density, which is the volume fraction of the particles, is $\rho = n \cdot V_{sphere}/V_{tot}$, with $V_{sphere} = 4\pi R^3/3$. Rearranging the above relation gives us:

$$\frac{V_{tot}}{n} = \frac{4\pi}{3\rho} R^3. \tag{2.7}$$

Assuming that the liquid with volume V_l distributes itself completely in the capillary bridges, the volume V of one bridge can be determined by $V = V_l/(n \cdot N/2)$. The average number N of liquid bridges per sphere will be discussed in more detail further below. Using the definition of the liquid content $W = V_l/V_{tot}$ and eq. 2.7 one can determine V^*:

$$V^* = \frac{V}{R^3} = \frac{1}{R^3} \cdot \frac{2V_{tot}W}{nN} = \frac{8\pi W}{3\rho N}. \tag{2.8}$$

As one can see from eq. 2.5 and 2.6, the energy that is being dissipated during a bridge rupture is proportional to the square root of the liquid content.

All in all, adding a wetting fluid to a sample of dry granular matter causes two fundamental changes:

1. Due to the formation of capillary bridges the sample becomes stiffer. The particles are pulled towards each other by the capillary force, which is an attractive as well as a hysteretic force.

2. An additional source of energy dissipation arises: the rupture of a liquid bridge. Later in this thesis it will be shown that the amount of energy which is being dissipated during that process can be used as an appropriate scaling factor of the energy of the system.

2.1. Dynamical phase transitions

In order to get further insight into the dynamical behavior of wet granular matter, the sample can be shaken vertically. In the following, previous results of Huang et al. [11] will be summarized.

The applied vibration is sinusoidal, i.e., the time-dependent height h of the container can be described by $h(t) = A\cos(\omega t)$. Small glass beads are wetted by a liquid and put into a flat petri dish. Due to the sinusoidal movement, the sample experiences an acceleration $a(t) = \ddot{h}(t) = -A\omega^2\cos(\omega t)$. With the definition of the angular frequency $\omega = 2\pi f$, the following quantity is introduced:

$$\Gamma := 4\pi^2 A f^2 \,/\, g. \tag{2.9}$$

Hence, Γ is the dimensionless maximum acceleration the system is exposed to, scaled with the gravitational acceleration g. What is more, the maximum velocity of the container walls is $v_{max} = 2\pi Af$. Another system-relevant quantity is:

$$E^* := \frac{1}{2} m v_{max}^2 \,/\, \Delta E_{cap}. \tag{2.10}$$

This dimensionless quantity is the kinetic energy of a bead with mass m and the maximum velocity of the container bottom, scaled with the bridge rupture energy ΔE_{cap} (see eq. 2.5). Γ and E^* can be varied by changing the frequency f and the amplitude A of the sinusoidal oscillation. They are identified as the two control parameters, which characterize the dynamics of the system.

By varying those two parameters, several phase transitions of the sample can be observed. Referring to systems in thermodynamic equilibrium, three phases in which the wet granular matter can reside in are identified as follows: solid (S), fluid (F) and gaseous (G). A coexistence between the fluid and gaseous state (C) is possible as well. It is an astonishing finding however, that a system far from thermal equilibrium can also reside in different phases and thus undergo phase transitions from phase (i) to phase (j). In the case of wet granular matter this behavior is due to the balance between injected energy and the energy dissipation which is dominated by ruptures of capillary bridges. Note that permanent injection of energy is essential for the system under study. Otherwise one would not see different phases, but rather one final cluster of unmoving particles connected by capillary bridges.

Fig. 2 shows a typical phase diagram with the control parameters Γ and E^* as variables. At low accelerations, $\Gamma \lesssim 1$, the particles experience a purely downward force, because the gravitational acceleration is larger than the externally applied one. Thus, the particles follow the vertical sinusoidal movement, but they don't move around within the container. This state is defined as the solid state.

For $\Gamma \approx 1.9$ a phase transition from solid to fluid is observed (using water as the wetting liquid): The particles start to move around relative to each other. As can be seen in fig. 2, the transition seems to be independent of the energy transferred into the system. That is the reason for calling this transition force driven (the force is proportional to the acceleration). The phase transition was observed in a dry granulate as well, but for lower accelerations ($\Gamma \approx 1.2$). The difference between the dry and wet case supports the idea of an enhanced mechanical stability of the sample which is caused by the formation of capillary bridges.

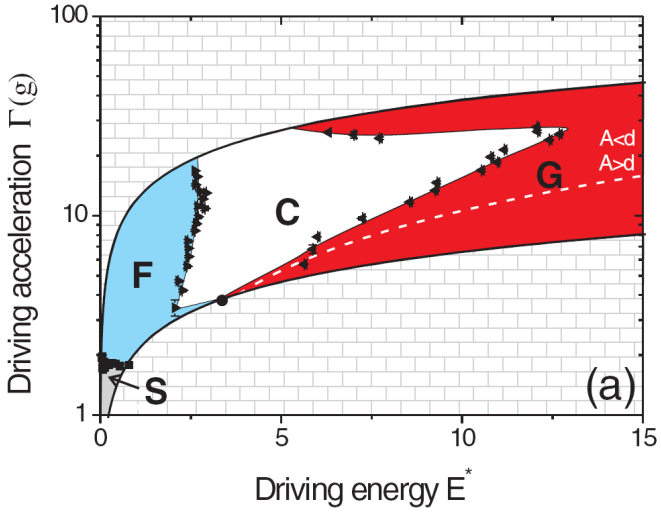

Figure 2: Phase diagram of a wet granular matter (glass beads and water) obtained by experiments [11]. The colors indicate the different phases: solid (S) in gray, fluid (F) in blue, fluid-gas coexistence (C) in white, and gas (G) in red. The liquid content is $W = 0.01$, and the bead diameter $d = 1.5\,\mathrm{mm}$. The image is reprinted with permission.

Crossing a certain energy E_c^*, a 'gas bubble' emerges and is in coexistence with the fluid phase. The gas bubble is less dense than the fluid and the glass beads seem to move faster. In order to get a better picture of this coexistence, a look at fig. 3 might help. This time, the transition (F)-(C) is independent of the acceleration and is therefore called energy driven. It should be noted that the coexistence region can only be reached if the acceleration is high enough as well. Simulations of wet granular matter under vertical agitation were also carried out [8]. The authors report the existence of a gas bubble, and were able to show that the granular temperature between the fluid and gas phase differs by an order of magnitude of two. Thus, the system is indeed in a state far from thermodynamic equilibrium.

A third transition (C)-(G) occurs once the gas bubble has pushed away the fluid, i.e., the density difference between fluid and gas has vanished and the sample occupies the whole container. According to a mean-field model [8], this transition line should parallel the (F)-(C) boundary, which is not the case in fig.2. Apparently the transition is more complex and might also depend on the experimental setup.

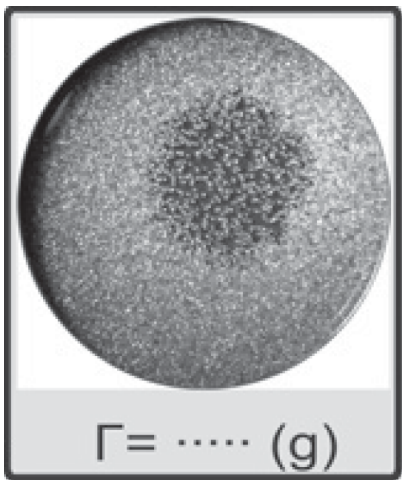

Figure 3: The gaseous phase is in coexistence with the fluid phase and expresses itself in a round gas bubble that is less dense than its surroundings. The picture was taken by Huang et al. [11] in earlier experiments and is reprinted with permission.

2.2. Variation of liquid content

As we have just seen in the previous section, adding a certain amount of liquid to a dry granular matter has the formation of liquid bridges as a consequence. This is, however, only true for a limited range of liquid contents. According to Herminghaus [10], there is a lower boundary around 10^{-3} due to the roughness of particles in a real system. Furthermore, the regime of capillary bridge formation is bounded by an upper value. This boundary (in the following denoted as W') occurs when too much liquid is present in the system, causing the single capillary bridges to coalesce. This in turn leads to the formation of different liquid clusters. While there has been paid some attention to the lower boundary (see for example [10]), changes in the mechanical stability of wet granular matter for higher liquid contents (i.e., $W > W' \approx 0.024$) were addressed only recently [15].

Let us first take a look at the average number of capillary bridges per particle. It is intuitive to first consider the packing geometry and the resulting number of nearest neighbors (coordination number N_c) for a dry granulate. The earliest study revealed an average number of $N_c = 6.4$ [3]. Taking numerous results from different research groups into account, one can say that the average lies in the range $N_c \in [4.8, 6.4]$ [10]. Since capillary bridges can also exist between two spheres which are not in contact, the average number N of capillary bridges per sphere may differ from the

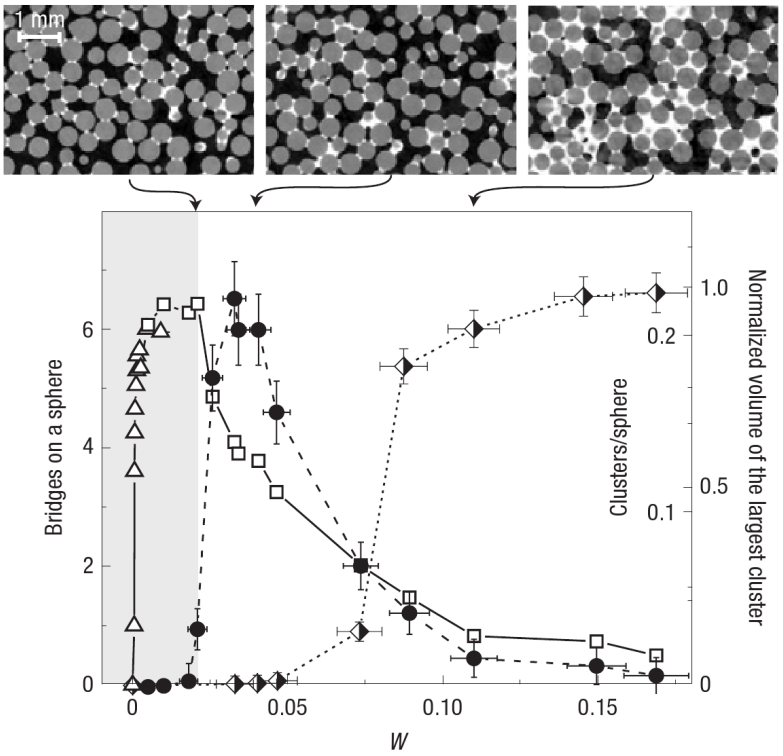

Figure 4: The images show cross sections of 3D tomograms at W=0.02, 0.04 and 0.11 from left to right. The main panel displays the average number of capillary bridges per sphere (open triangles and squares), the average number of clusters per sphere (filled circles), and the normalized volume of the largest cluster (half-filled diamonds). The figure is taken from Scheel et al. [16]

coordination number.

Scheel et al. [16] performed X-ray microtomography experiments with a variety of glass beads wetted with an aqueous zinc iodide solution in order to be able to count N for several different liquid contents. Fig. 4 displays their results. At this point, the definition of a capillary bridge should be made clear: A capillary bridge is defined as a liquid domain being in contact with exactly two neighboring particles. Adding more and more liquid to the system, the volume of a capillary bridge increases, and the bridge is growing. At one point, the capillary bridges on one sphere have become so large that they touch and coalesce. As can be seen in fig. 4, the regime of the liquid content in which individual capillary bridges exist ends at $W' \approx 0.024$ [15]. Until that point, about 6.4 capillary bridges exist per bead. The sharp rise at low liquid contents is due to the lower boundary which was mentioned in the beginning of the section. The coalescence of capillary bridges, and thereby forming new liquid

clusters, continues with a rising liquid content until all of the liquid is combined in one big cluster (at $W \approx 0.11$ the largest cluster already contains about 90% of the liquid [15]).

In conclusion, the morphology of the liquid distribution changes drastically when increasing the liquid content: Starting from single capillary bridges which are merging to one final continuous cluster. A statistical analysis of the data obtained by X-ray tomography revealed that at higher liquid contents, $W > W'$, so-called trimers can be found abundantly in the sample. Consider three capillary bridges which are connecting three neighboring particles. When the bridges start to touch each other they enclose a hexagon of air in between them. Once this void is filled, the configuration is termed a trimer (see fig. 5(a)).

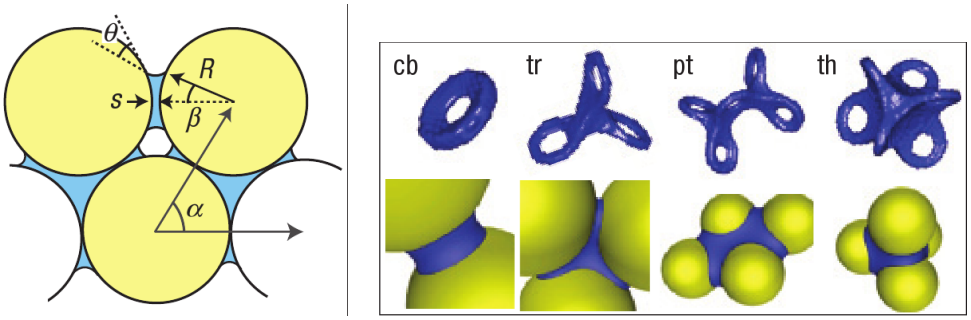

(a) sketch of one capillary bridge in comparison to two trimers

(b) Displayed are: capillary bridge (cb), trimer (tr), pentamer (pt), tetraheda (th) (as obtained from X-ray tomography)

Figure 5: Different liquid clusters found in wet granular matter. Both Figures are reprinted from Scheel et al. [15] with permission.

While a single liquid bridge is growing, the absolute value of the Laplace pressure which was introduced as the pressure difference Δp earlier (see eq. 2.1) is decreasing. However, on average a liquid bridge cannot have a half-filling angle $\beta > 30°$, since at that point two liquid bridges coalesce (it is presumed that there are always six bridges on one glass bead, which is in accordance with the data plotted in fig. 4). According to Scheel et al. [15], the Laplace pressure at $\beta = 30°$ is:

$$\Delta p^* \approx -4.46 \frac{\gamma}{R}, \tag{2.11}$$

where γ is the surface tension and R the radius of the glass spheres. Perfect wetting of the glass beads was assumed, i.e., the contact angle between the liquid and

the sphere is zero. The authors argued that whenever the volume of a capillary bridge has increased so much that the corresponding Laplace pressure reaches Δp^*, it coalesces with two other bridges and the Laplace pressure will not increase further (the trimer is expected to have approximately the same mechanical strength of three individual bridges), but stay constant. Eventually the trimers will merge to different clusters when the liquid content is continuously being increased. So-called pentamers, heptamers, and so on are formed as a consequence (see fig. 5(b)). The morphology of the final cluster, which eventually contains all the liquid, resembles therefore an ensemble of many coalesced capillary bridges with a very large surface-to-volume ratio. Scheel et al. [15] measured the Laplace pressure experimentally and indeed, once the coalescing regime was entered at $W' \approx 0.024$, the pressure stayed constant (see fig. 6).

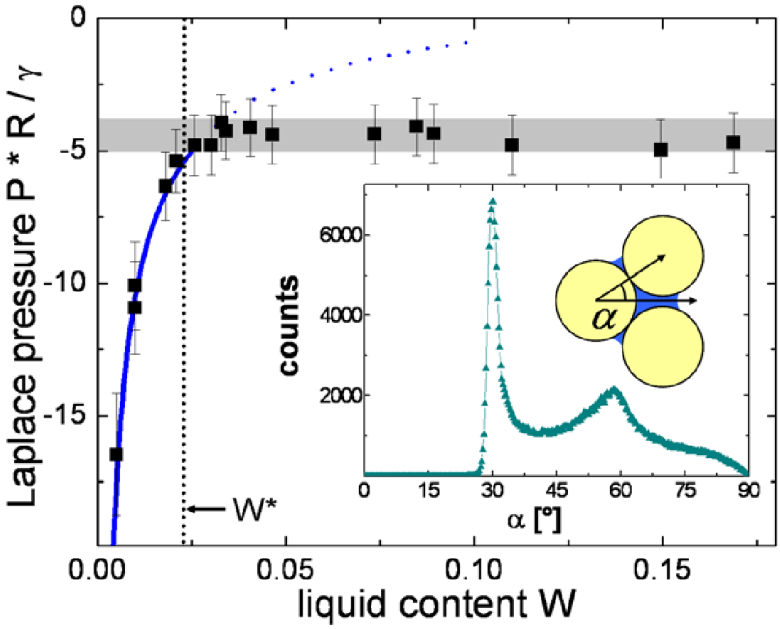

Figure 6: The Laplace pressure is normalized with the surface tension and bead radius. The squares were obtained experimentally. The solid (dotted for $W > W'$) line represents the calculated Laplace pressure of one single capillary bridge if it was able to grow without limitations (for complete wetting). The gray bar indicates the values of Δp^* for contact angles $0° \leq \theta \leq 10°$. Inset: Distribution of angular distances between two neighboring contact points and a sketch of a trimer.

The inset of fig. 6 is the quantification of the above statement that trimers seem to be numerous in a sample of randomly packed glass beads. All angular distances between two neighboring contacts have been counted by looking at the tomograms and then plotted. Clearly, there is a sharp peak at 30°, and angular distances smaller than 30° are not present at all.

One can conclude that, although the single capillary regime is left at higher liquid contents, the resulting liquid clusters exert similar forces on the particles. This was shown experimentally by measuring the Laplace pressure as a function of the liquid content. In the beginning of this section it was argued that the formation of capillary bridges introduces an increased mechanical stability to granular matter. When adding more liquid, this mechanical stability can apparently still be described by individual capillary bridges even though they are not present in the system anymore, because they have become part of new aggregates. The question that arises at this point is the following. How does the increase of the liquid content, and therefore the change of the morpholgy of the system, affect the dynamical phase transitions described in section 2.1? This is the central question which will be dealt with in this thesis.

3. Experimental setup

Fig. 7 illustrates the experimental setup used in this thesis. Small glass beads with a diameter of $1.4\,\mathrm{mm} \leq d \leq 1.6\,\mathrm{mm}$ and density $\rho = 2500\,\mathrm{Kg/m^3}$ served as the granular matter. The glass beads were obtained from "Mühlmeier GmbH & Co. KG", and 90 % of the beads are supposed to have a diameter in the above mentioned range. Due to this polydispersity, additional effects due to crystallization were eliminated. The beads were put into a flat petri dish (with a diameter of 145 mm) made out of glass. In addition, the dish is completely covered by a second petri dish, which has a slightly smaller diameter than the bottom one. This allows the top dish to slide into the bottom dish. The separation H between the bottom and top dish determines the total container height and can be adjusted by clamps and set screws. At all times, both dishes move together as a unit. Pictures of the setup can be found in Appendix C (fig. 23-25). Furthermore, an O-ring between the outer and inner perimeter of the top and bottom petri dish prevented the glass beads and the liquid to leave the container. In order to ensure reproducible results, both the glass dishes and the glass beads were cleaned using the same protocol before every measurement (see Appendix, A).

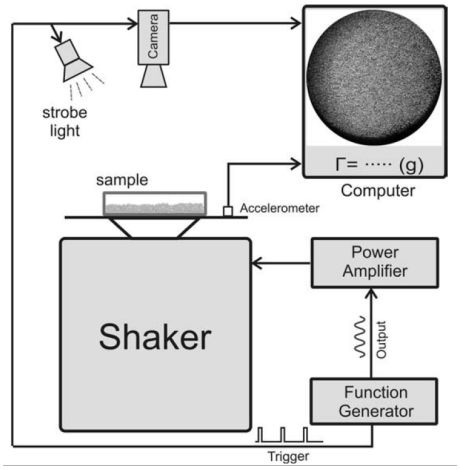

Figure 7: Experimental setup used in this thesis. Details of the setup can be found in the text. The figure is reprinted from Huang et al. [11] with permission.

According to the data sheet, the pile of glass beads has a bulk density $\rho_{bulk} = 1600\,\mathrm{Kg/m^3}$. Before every measurement, the weight m of a clean sample of glass beads was measured with a precision balance. The volume V_{tot} of the sample can therefore be obtained by dividing the weight m by the bulk density ρ_{bulk}. The volume V_{liquid} of the fluid was determined in the same way, whereas the density $\rho_{oil} = (913 \pm 2)\,\mathrm{Kg/m^3}$ was used (see Appendix, B). Finally, the liquid content is:

$$W = \frac{V_{liquid}}{V_{tot}} \tag{3.1}$$

	surface tension γ in $\left[\frac{\text{mN}}{\text{m}}\right]$	viscosity ν in [cSt]
distilled water	72.75	1.0
silicon oil	19.2	5.0

Table 1: Properties of the liquids used in this thesis. The values for water are taken from [18] at the temperature 20° C and for silicon oil from [9] at the temperature 25° C.

Two different liquids were used: distilled water and silicon oil. The later was obtained from "L. Böwing GmbH". Important properties of those liquids are summed up in table 1.

The petri dish containing the wet granular matter was mounted onto an electromagnetic, and vertical shaker (TIRA TV5880/LS). A function generator (Agilent 33210A) generated a sinusoidal signal, which was amplified and drove the shaker. The acceleration was measured with an accelerometer (Kistler 8702B100M1), which was mounted directly to the bottom plate holding the petri dish. The signal coming from the accelerometer was measured with a voltmeter.

In order to determine the phase diagram discussed in section 2, one needs to note the frequency and the acceleration at which each phase transition takes place. Before the actual measurement, one needs to ensure the complete mixing of glass beads and liquid. This was accomplished by shaking the sample with a relatively small frequency ($f \approx 20\,\text{Hz}$) and a high acceleration ($\Gamma \approx 4-6$) for several minutes. Once the liquid was uniformly distributed, a constant frequency ($f \geq 60\,\text{Hz}$) was applied and the amplitude slowly increased. First, the sample was completely fluidized. The amplitude was then lowered until no motion of the glass beads could be detected anymore. The corresponding data pair (frequency and acceleration) denoted the phase transition between the solid and the fluid phase. Next, the amplitude was raised again until a stable gas bubble was visible. The frequency and acceleration were noted again. Finally, the frequency and acceleration defining the phase transition between the fluid-gas coexistence and gas phase were determined. This transition was characterized by a completely gaseous sample, i.e., the gas bubble had vanished and the rapidly moving glass beads occupied the whole container.

The whole process was repeated for several different frequencies ($60\,\text{Hz} \leq f \leq 130\,\text{Hz}$ in $\Delta f = 5$ Hz steps). Since the purpose of this thesis is to solely investigate the effect of a varying liquid content, all other parameters were kept constant.

Above all, the same container height $H = (9.00 \pm 0.05)$ mm and sample volume $V_{tot} = (70.0 \pm 0.1)$ ml were used throughout the experiments.

4. Results

4.1. Water as the liquid

At first, distilled water was the liquid of choice, since it wets the glass beads almost perfectly. Thus, the contact angle θ between the liquid-gas interface and a bead is nearly zero. The properties of distilled water are listed in table 1. While trying to determine a suitable set of parameters (i.e., container height H, sample volume V_{tot}, frequency range), it was observed that it was nearly impossible to obtain reproducible data. The onset of the fluid-gas coexistence as well as the gaseous phase varied by up to 20%, although all parameters were kept constant. A first attempt to solve this problem concerned the cleaning protocol of the glass beads as well as the container (see Appendix, A). It was the aim to ensure equal initial conditions, but the outcome was nevertheless not satisfactory. Even during a single measurement the onset of the phase transitions was not consistent. The longer a measurement lasted, the earlier the gas bubble nucleated. This observation eventually led to the explanation of the problem. A close inspection of the container lid under a microscope revealed that the glass beads seemed to crumble during a measurement. Fig. 8 shows an image of the lid, which was directly taken after a measurement. The surface seemed to be covered with some kind of dust, which could easily be wiped away with a needle (the long bright strip shows the region which was cleared of the dust). Clearly, the fine particles making up the dust had to stem from the glass beads. According to the data sheet [13], the breaking resistance of the beads is $2.380\,\mathrm{N/mm^2}$. This corresponds to a force of approximately $140 \cdot g$, where $g = 9.81\,\mathrm{m/s^2}$ denotes the gravitational acceleration. Therefore, the force exerted on the glass beads by the vertical agitation is not sufficient to damage the glass beads [1].

It is well known, that reactions between water and glass can eventually lead to corrosion of the latter (see for example [4, 6]). The glass beads used in this thesis are made out of soda-lime glass, which consists of 60-70% silica (SiO_2). The surface of glass is never perfectly smooth, but it is rather rough and microscopic cracks are present. Basically, water molecules react with the silicon-oxygen bonds of the glass and thereby split up the latter. If a small crack is present, this reaction causes the crack to grow. Under normal circumstances the reaction takes place on a very long time scale, and therefore silica is usually not prone to corrosion caused by water. If,

[1] The highest exerted force has been $50 \cdot g$, which is well below the breaking limit

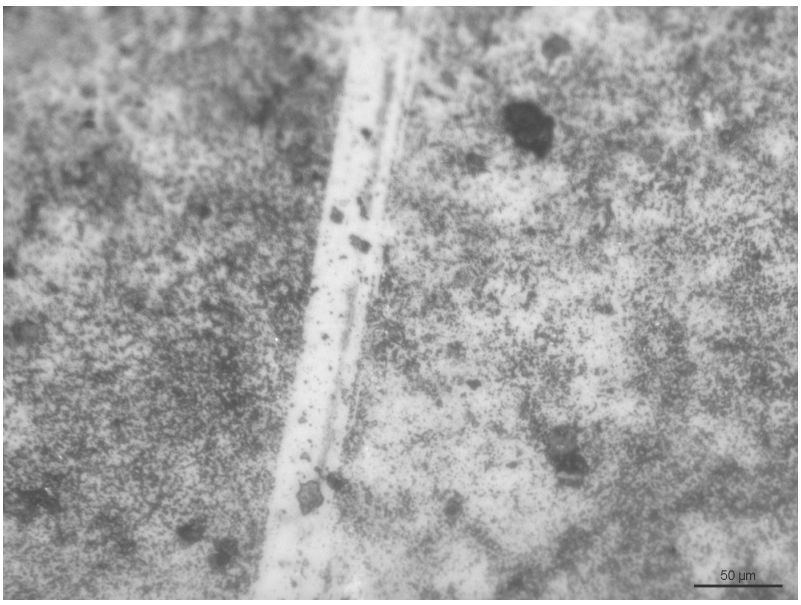

Figure 8: The image was obtained by a microscope. Displayed is the glass lid of the container after a measurement. Note that the scale bar on the right side on the bottom represents 50 μm .

however, a great stress is present, the crack growth is accelerated by the reaction with water. This can ultimately lead to failure.

In conclusion, the combination of using water as a wetting liquid and applying a vertical agitation with a high acceleration might have repeatedly damaged the glass beads during impacts with the container walls as well as with each other. Therefore, the granular sample did not solely consist of macroscopic and spherical glass beads anymore, but very small and non-spherical glass particles (which are seen as dust on the lid of the container) were present as well. This changed the properties of the wet granular matter drastically, since the surface area of the glass was greatly increased. The small particles literally soaked up the water. Hence, the effective amount of liquid forming liquid bridges between the original glass beads became less during a measurement and this affected the onset the phase transitions. Furthermore, the data could not be reproduced, since the corrosion of the glass beads is not predictable. Therefore, the composition of the sample was different from measurement to measurement.

Thus, replacing the water with another liquid, which does not interact with glass, might enable the glass beads to remain undamaged during collisions. Indeed, taking a look at the container lid after a measurement performed with silicon oil, which

wets glass perfectly as well, showed a clean surface. Moreover, the behavior of the sample did not change anymore. Above all, the onset of the phase transitions was reproducible.

4.2. Silicon oil as the liquid

4.2.1. Construction of a phase diagram

As was described in section 2.1, a system of glass beads mixed with a wetting liquid undergoes several phase transitions when applying a sinusoidal vertical vibration with amplitude A and frequency f. In this case, the wetting liquid was silicon oil with the properties listed in table 1 on p. 15. For convenience, the phases of the system and its abbreviations can be found in table 2. A phase transition from one phase (i) into another phase (j) will be denoted by (i)-(j).

In the following, the construction of the phase diagram with the variables

$$\Gamma = 4\pi^2 f^2 A \,/\, g \qquad \text{and} \tag{4.1}$$

$$E^* = \frac{1}{2} m (2\pi f A)^2 \,/\, \Delta E_{cap} \tag{4.2}$$

will be described. As an example serves the measurement with the liquid content $W = 0.0795 \pm 0.0002$. The phase diagrams for the remaining liquid contents have been constructed exactly in the same way. Once a phase transition was observed in the experiment, the corresponding frequency f and acceleration a of the sinusoidal vibration were noted. The acceleration was measured by an accelerometer with a sensitivity of $s = 49.76\,\mathrm{mV}/g$ ($\pm 5\%$) [12] and a voltmeter (measuring the root mean square voltage of the signal coming from the accelerometer).

Phase	Abbreviation
Solid	(S)
Fluid	(F)
Fluid-Gas Coexistence	(C)
Gas	(G)

Table 2: Noted are the abbreviations of the observed phases of the wet granular matter.

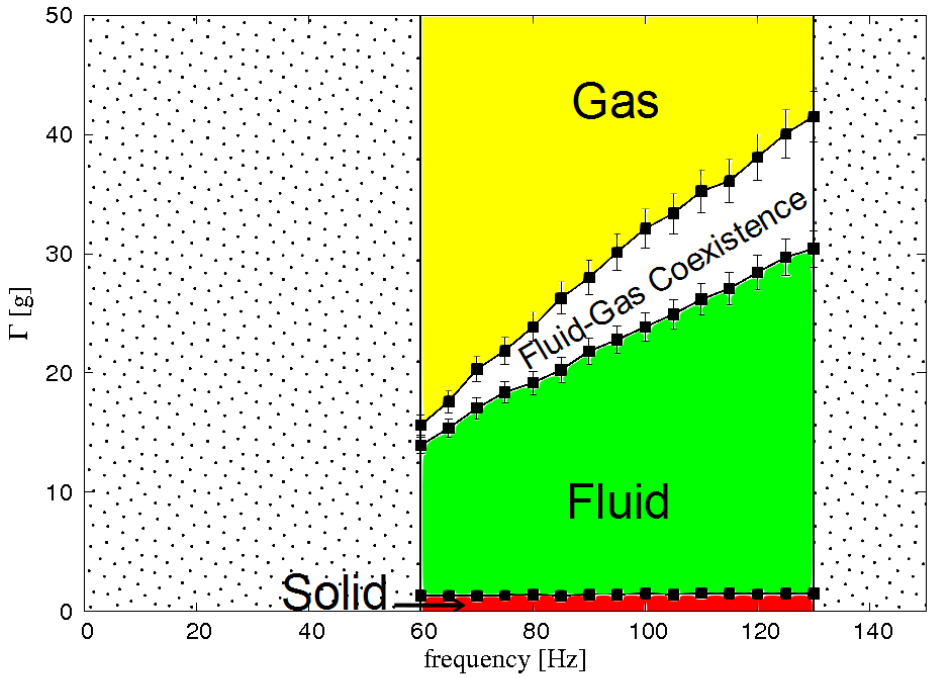

Figure 9: Phase diagram of glass beads wetted with silicon oil at the liquid content $W = 0.0795$ spanned by the externally applied frequency and the peak acceleration. Each square represents the measured data pair (f, Γ) when a phase transition took place. The colored regions correspond to the different phases of the system: solid (red), fluid (green), fluid-gas coexistence (white) and gas (yellow). The unexplored region is depicted by black dots.

Fig. 9 displays the result, whereas $\Gamma = a\,/\,g$ was plotted versus f. It should be noted that only the colored regions were explored experimentally. In order to ensure that the applied amplitude was reasonably smaller than the diameter of the glass beads at all times, frequencies $f \geq 60$ Hz were considered. In this way, unwanted geometrical effects could be neglected. The upper boundary ($f = 130$ Hz) was determined by the apparatus: The higher the liquid content, the higher the acceleration which had to be applied in order to drive the system into the gaseous phase. At such high accelerations the O-ring between the bottom and upper part of the container (preventing the glass beads and the silicon oil from leaving the container), started to slip. As a consequence, the silicon oil began to creep out of the container and the liquid content could not be kept constant any longer. The

vertical error bars in fig. 9 are estimates which mainly represent fluctuations of the reading of the voltmeter. The fluctuations increased considerably once the gas bubble appeared, since the bouncing of the glass beads against the container influenced the accelerometer. In addition, the uncertainty of the accelerometer was taken into account. The frequency was considered to be exact.

When taking a look at the above phase diagram, one notices that the phase transition (F)-(C) is displayed by a straight line, i.e., $\Gamma \,/\, f$ seems to be constant. Let us take a closer look at this (considering eq. 4.1 as well):

$$\frac{\Gamma}{f} = \frac{4\pi^2 f^2 A}{fg} = \frac{2\pi}{g} \cdot v_{max}, \tag{4.3}$$

where $v_{max} = 2\pi f A$ is the maximum velocity of the container walls. Thus, it is an interesting task to plot Γ versus v_{max} as was done in fig. 10. The velocity was obtained from the measured data by the following relation:

$$v_{max} = \frac{\Gamma \cdot g}{2\pi f}. \tag{4.4}$$

The error $\sigma_{v_{max}}$ of the peak velocity was calculated by propagation of uncertainty [1]. As expected, the phase transition line is more or less a vertical line in the Γ-v_{max} plane. This, in turn, means that the gas bubble occurs only, when the walls of the container have a certain peak velocity v_c.

In general, a velocity of a particle with mass m can be linked to its kinetic energy by $E = 1/2mv^2$. Plotting Γ versus the kinetic energy $E_{wall,\,max} = 1/2mv_{max}^2$ (i.e., only those glass beads, which have the velocity v_{max} of the container are taken into account) resulted in a new phase diagram which has two very fundamental quantities as variables: energy and force (the force is directly proportional to the acceleration). In addition, $E_{wall,\,max}$ was normalized by the energy which is dissipated when a capillary bridge ruptures:

$$\Delta E = 5.5\gamma R^2 \sqrt{\frac{8\pi}{3}\frac{W}{\rho N}}, \tag{4.5}$$

as can be seen when combining eq. 2.5 and 2.6 (silicon oil completely wets the glass beads, i.e., $\cos(\theta) = 0$). The mean radius of the glass beads stayed constant throughout the experiments: $R = 0.75\,\mathrm{mm}$. Assuming a random dense packing, one

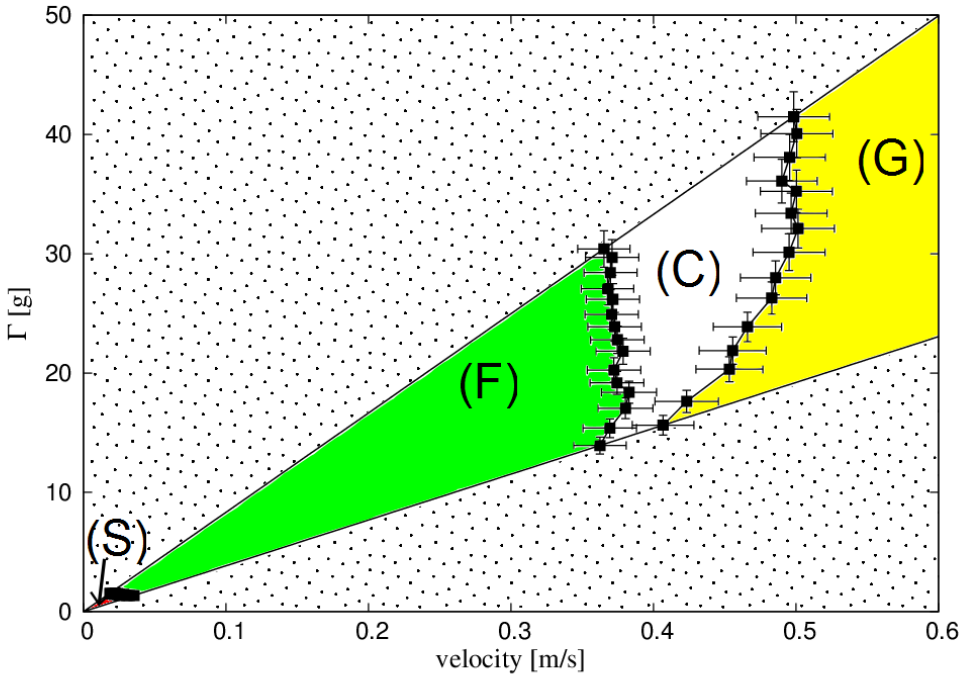

Figure 10: Phase diagram of glass beads wetted with silicon oil at the liquid content $W = 0.0795$ spanned by the peak velocity and the peak acceleration of the container walls. The color code is identical to the one in fig. 9

obtains the packing density $\rho = 0.62$ [10] and the silicon oil used in this thesis has a surface tension of $\gamma = 19.2\,\mathrm{mN/m}$. In accordance with section 2.2, an average number $N = 6$ of capillary bridges per bead was assumed. The relevance of the energy scaling will be discussed further below. Fig. 11 shows the final phase diagram. The error σ_{E^*} of the scaled energy was again computed by propagation of uncertainty [1].

4.2.2. General discussion of the phase diagram

In this section, general aspects which can be seen in the just obtained phase diagram will be discussed. Although it will be referred to fig. 9 - 11 at all times, the observed phenomena are present in every phase diagram (independent of the liquid content). First of all, fig. 9 shows clearly, that the onset of fluidization is depicted by a horizontal line. Apparently, the phase transition (S)-(F) does not depend on the frequency, but only on the acceleration. Taking a look at the inset displayed

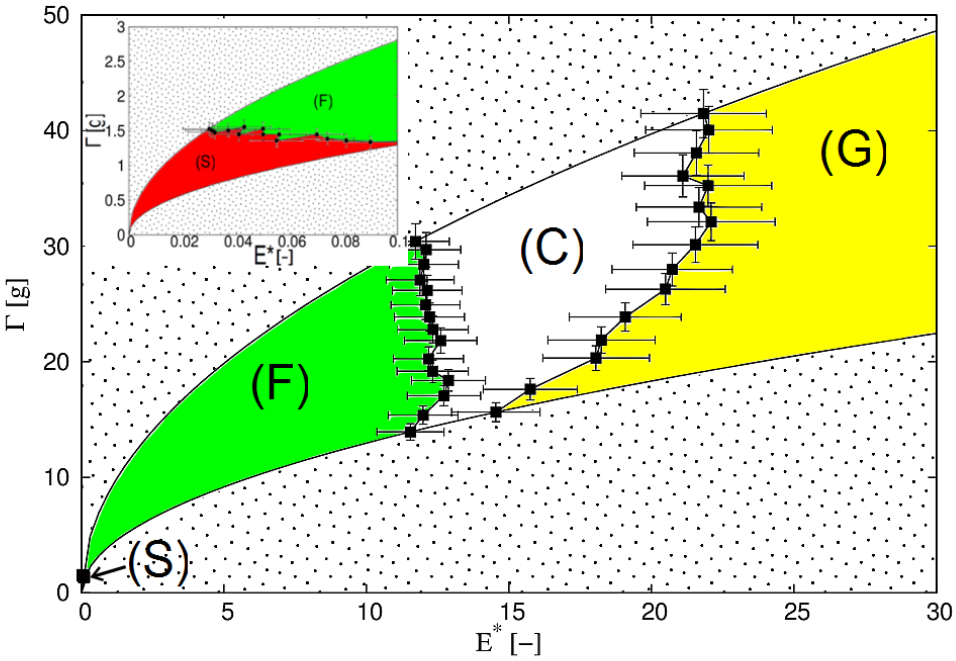

Figure 11: Phase diagram of glass beads wetted with silicon oil at the liquid content $W = 0.0795$ spanned by the dimensionless energy E^* and the peak acceleration of the container walls. The color code is identical to the one in fig. 9. The inset shows a magnification of low energies E^* in order to make the phase transition (S)-(F) visible.

in fig. 11 illustrates that this phase transition does not depend on the energy injected by the walls either. The critical acceleration at which fluidization sets in is $\Gamma_c = 1.45 \pm 0.03$. This value represents the weighted mean of the data points forming the horizontal line in fig. 9. The result is in good agreement with earlier experiments (e.g., Huang et al. [11]), although the authors reported a critical acceleration of $\Gamma_c \approx 1.9$. The difference could stem from the use of different liquids: While Huang et al. [11] used distilled water with the surface tension $\gamma = 72.75\,\mathrm{mN/m}$, the wetting liquid of choice in this thesis is silicon oil with $\gamma = 19.2\,\mathrm{mN/m}$. As can be seen from eq. 2.3, the capillary force is directly proportional to the surface tension. Since the latter is smaller in the case of silicon oil, the force needed to overcome the capillary force and hence enable a bead to move relative to its neighbors is smaller as well. This finding coincides with earlier experiments obtained by Scheel et al. [17], who found Γ_c to be proportional to the surface tension of the liquid.

Next, the appearance of the gas bubble will be discussed in more detail. Fig. 12 displays the nucleation of a typical gas bubble as it was observed throughout the experiments. It started out as a small fluctuation and grew until it was stable at a certain size. Note that the bright dot in the middle of the gas bubble in the last picture is not part of the fluid phase (it is a screw which was used to bolt down the bottom plate to the shaker). Since the gas bubble appeared at random positions within the sample when repeating the measurement, an inhomogeneity in the apparatus or the excitation amplitude could not account for the existence of the gas bubble. The onset and behavior of the fluid-gas coexistence changed somewhat when increasing the liquid content. A closer look at that will be taken in section 4.2.4. Despite the differences, however, the shape of the curve depicting the phase transition (F)-(C) in fig. 11, does not change qualitatively in the phase diagrams obtained at different liquid contents. Clearly, the phase transition is represented by a more or less vertical line. Therefore, in contrast to the transition (S)-(F), the onset of the fluid-gas coexistence seems to be independent of the force. Thus, the driving mechanism in this transition appears to be the energy which is injected by the walls of the container. As it was described in section 2.1, the vertical transition line was observed by Huang et al. [11] as well.

In addition, it can be seen in fig. 11 that for low accelerations the transition line is not vertical. In this regime the phase boundary is rather represented by a rising curve. The cause of this initial deviation is still unknown, but it is peculiar that it is reproducible and has furthermore occurred for all liquid contents.

It is an interesting finding that the phase transition (F)-(C) takes place at a noticeable higher critical energy ($E_c^* = 12.2 \pm 0.4$) than it was reported by Huang et al. [11] ($E_c^* \approx 2.5$). This shift might be explained by the use of different liquids as well. On the one hand, the vertical phase transition line indicates that the glass beads need to have a minimum velocity v_{min}, and therefore a corresponding minimum energy E_{min}, in order to be able to break a liquid bridge. If the only source of energy dissipation in the system was indeed the bridge rupture, the minimum required energy would be $E_{min} = \Delta E_{cap}$. Hence, one would expect the transition line to occur at $E_c^* = E_{min} \,/\, \Delta E_{cap} = 1$. In the past, Röller [14] performed simulations concerning wet granular matter. Based on those simulations, phase diagrams with the variables E^* and Γ were constructed and compared to earlier experimental data. It was indeed observed that the phase transition (F)-(C) is a vertical line at

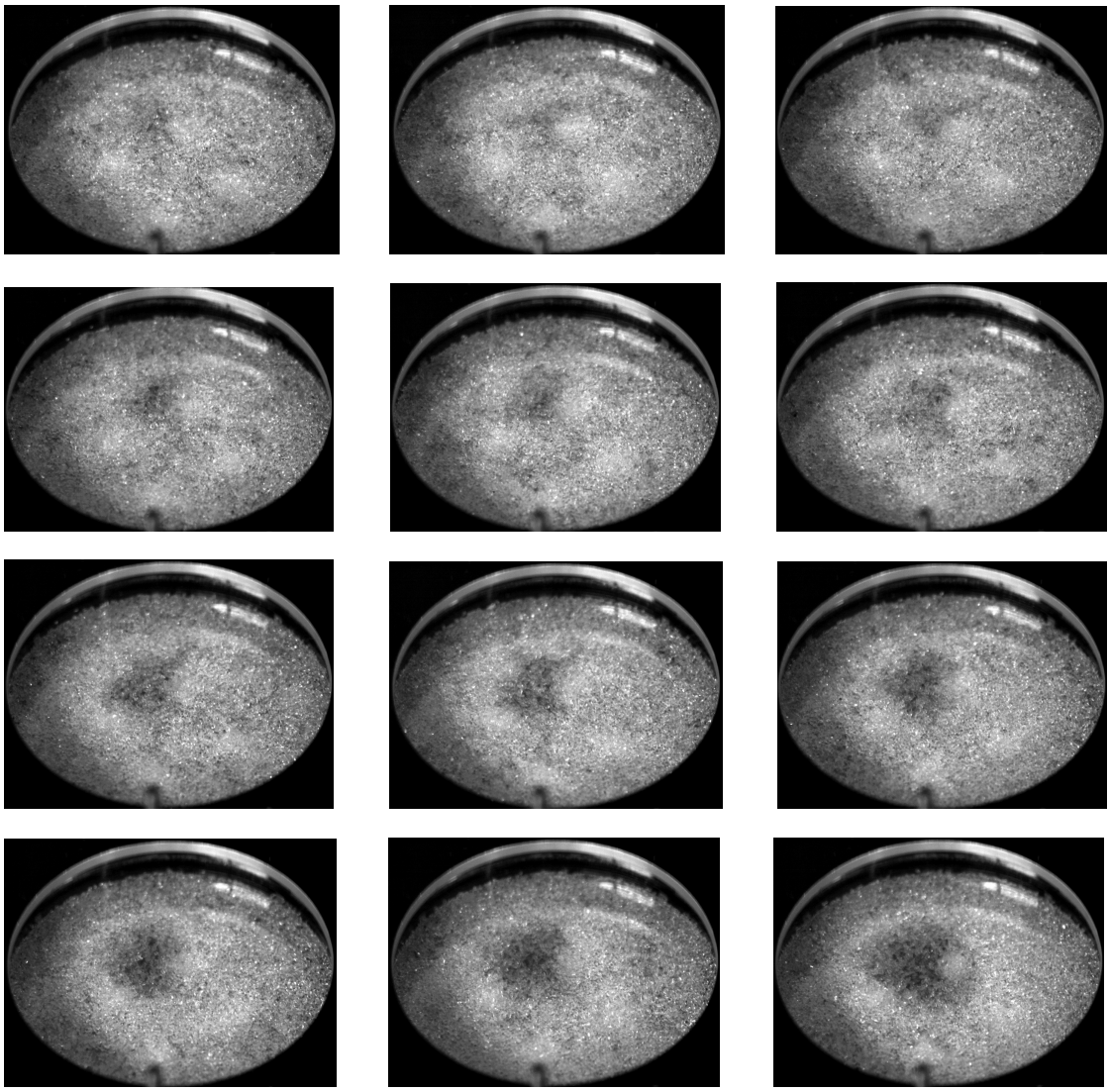

Figure 12: From left to right: Nucleation of a gas bubble at $W = 0.988 \pm 0.003$, $f = 60\,\mathrm{Hz}$ and $\Gamma = 14.8 \pm 0.8$.. The time elapsed between the first and the last image is 1.08 s.

$E_c^* = 1$ when *only* the bridge rupture energy was taken into account as a source of energy dissipation. Above all, the inelasticity of the collisions is neglected by making that crude assumption, i.e., in a real system more energy is dissipated due to inelastic collisions. Additional simulations incorporating the effects of inelasticity by introducing the coefficient of restitution ϵ (described in the beginning of section 2) were conducted by Röller [14]. Lowering ϵ to values of 0.8, a shift of the vertical line toward higher E^* was observed.

On the other hand, it was reported that the coefficient of restitution is altered in "wet collisions" [2, 10], i.e. when a liquid is present between two colliding particles. Amongst others, the viscosity of the liquid seems to affect ϵ: The higher the viscosity, the lower the coefficient of restitution. In other words, more energy is dissipated in a collision between two particles once a liquid with a higher viscosity is inserted between said particles. Therefore, the particles need to have even more energy in order to break a liquid bridge, which is thought to be the requirement for the onset of the fluid-gas coexistence. Since the silicon oil used in this thesis is five times more viscous than water (refer to table 1), a significant shift of the phase transition line toward higher energies is to be expected[2]. Further experiments using liquids with different viscosities would have to be conducted in order to test this qualitative argument.

The critical energy E_c^* could also be affected by the experimental setup. As was reported by Huang et al. [11], the diameter and height of the container and especially the filling height of the sample might contribute to the shift toward higher energies.

The fluid-gas coexistence occupies a fairly large region in the phase diagram. It is bounded by a second phase transition line which denotes the onset of a homogeneous gas phase. Until then, the size of the gas bubble increases and gradually pushes the fluid phase aside. Finally, the density difference between the two phases vanishes. Crossing that transition line therefore means that the energy of the glass beads is so high that every collision is followed by a bridge rupture. The shape of this transition line depends to a larger degree on the liquid content than the two previous ones. Nevertheless, all phase diagrams share the following features. For low accelerations, the transition line (C)-(G) starts close to the transition line (F)-(C). Instead of being a vertical line, the curve exhibits a steady rise at first. Eventually the line becomes vertical. It should be noted that the vertical part of the transition line is not always as prominent as in this example. As was already mentioned in section 2.1, a simple mean-field model predicts a vertical transition line. Phase diagrams obtained by simulations from Röller [14] show a vertical line for higher accelerations as well. Another region of fluid-gas coexistence appeared in the simulations, once inelasticity was taken into account. One such phase diagram, obtained

[2]The capillary number $Ca = v_0\eta\,/\,\gamma$ describes the ratio of the viscous force to the capillary force. Here, v_0 denotes the relative velocity of the glass beads, η is the dynamic viscosity and γ the surface tension of the liquid respectively. Assuming a velocity of $v_0 = 0.3\,\mathrm{m}\,/\,\mathrm{s}$, one gets $Ca \approx 0.004$ in the case of water and $Ca \approx 0.072$ for silicon oil.

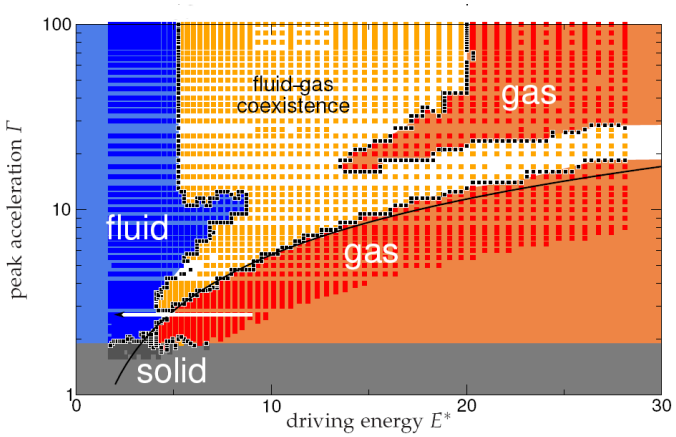

Figure 13: Phase diagram obtained by simulations with a coefficient of restitution $\epsilon = 0.8$. The colored regions correspond to the different phases of the system: solid (gray), fluid (blue), fluid-gas coexistence (white) and gas (orange). The solid black curve denotes where the driving amplitude equals the diameter of the glass beads. The figure is reprinted from [8] with permission.

by simulations incorporating a coefficient of restitution of $\epsilon = 0.8$ is displayed in fig. 13.

The additional coexistence region is present for lower accelerations and is rather narrow. It was argued that this coexistence region is caused by inelastic effects, because it is absent in phase diagrams considering elastic collisions. Experimentally, data points in this part of the phase diagram can be obtained by applying higher driving amplitudes A of the vertical vibration (the amplitude increases when going from the upper left to the bottom right corner in the phase diagram). In fig. 13, the black curve, which appears to be a lower boundary of the additional coexistence region, represents the acceleration at which the driving amplitude equals the diameter of the glass beads. It should be noted, however, that the coexistence region does not necessarily have to coincide with the $A = d$ curve. It rather depends on numerous factors, such as filling height and bead diameter as well as the packing density.

Let us compare the phase diagram obtained experimentally (fig. 11) with the one obtained by simulations (fig. 13). Throughout the experiments, the driving amplitude was always smaller than 1 mm, i.e., $A < 2/3\,d$, where d denotes the bead diameter. The reasoning for choosing rather small amplitudes was already put forward earlier: geometrical effects were to be eliminated. Thus, it is plausible to assume that only one coexistence region, namely the upper one, shows up in the

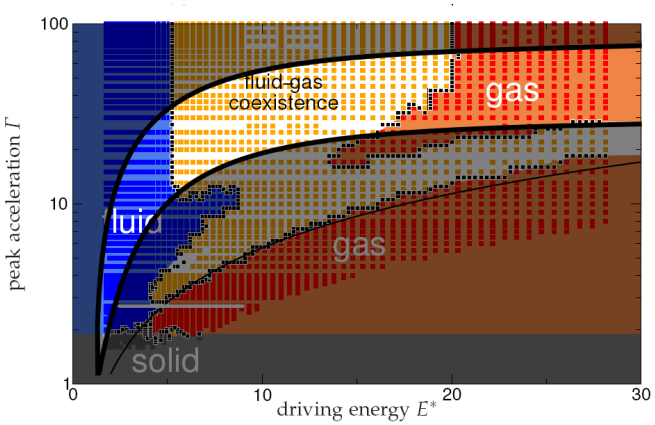

(a) Altered phase diagram obtained by simulations [14]. The parameters are the same as in fig. 13

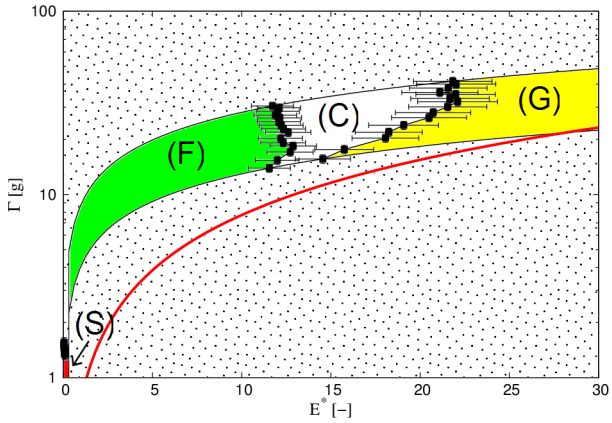

(b) Altered phase diagram obtained by experiments. The parameters are the same as in fig. 11

Figure 14: Shown is a comparison of two phase diagrams obtained by (a) simulations and (b) experiments. The alterations are explained in the text.

phase diagram obtained by experiments. In order to measure the other one as well, one would have had to apply larger amplitudes. A look on fig. 14 might clarify this argument. The experimental phase diagram is replotted on a log/linear scale and the $A = d$ curve is added in red. In addition, two black solid lines have been drawn into the phase diagram from [8]. The darkened regions correspond approximately to the unexplored (dotted) region of the experimental phase diagram in fig. 11. It should be pointed out that the darkened region is only depicted schematically. Comparing the two phase diagrams with each other, illustrates that very likely only

the upper coexistence region was measured experimentally. The other coexistence region, caused by inelastic effects, might be hidden in the "dotted" and therefore unexplored region. Taking this into account, the measured phase transition is in very good agreement with the simulations.

4.2.3. Effect of a varying liquid content on the phase transition (S)-(F)

The critical acceleration Γ_c at which fluidization sets in is not affected by increasing the liquid content W. This can be seen by plotting Γ_c against W. In the previous section it was already shown that the phase transition is independent of the frequency. Therefore, the weighted mean of Γ_c was computed for each phase diagram obtained at a different liquid content. Fig. 15 displays the result.

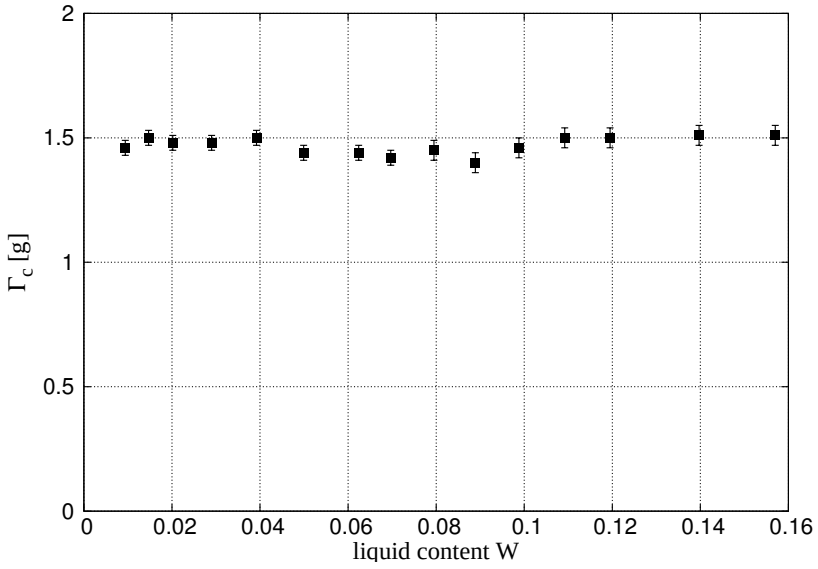

Figure 15: Shown is the dependence of the critical acceleration at which the sample is fluidized against the liquid content. Each data point represents the weighted mean of one phase diagram.

It should be noted that for liquid contents $W > 0.10$ the phase transition was harder to determine experimentally, because the larger liquid clusters would reorganize themselves, without an actual movement of the glass beads. Those two processes, the movement of a bead and reorganization of the liquid, can be easily confused. This was taken into account by adjusting the error bars toward higher values.

As was already described earlier, Γ_c corresponds to the force which is needed to overcome the capillary force. In addition, we have seen that the regime in which

single capillary bridges exist ends at $W' \approx 0.024$ (see sec 2.2). Nevertheless, the critical acceleration does not change for $W > W'$. This implicates, that the new liquid clusters (generated during the coalescence process of liquid bridges) exert similar forces on the glass beads, compared to the capillary force of a single bridge. This result is in good agreement with earlier experiments conducted by Scheel et al. [15].

4.2.4. Effect of a varying liquid content on the phase transition (F)-(C)

Visual changes

Just by looking at the sample during the measurements, three different regimes could be identified. The first one was observed for relatively small liquid contents, $W < 0.03$. Here, the gas bubble was only slightly visible. One could definitely hear the onset of the gaseous phase, because the glass beads were bouncing against the top of the container. This is in clear contrast to the fluid phase, in which the beads only move around in the bottom half of the container. Inspecting the sample closely, one was also able to see the gas, although not as prominent as for example in fig. 12. It seemed that the gas was on top of the fluid and thus hard to see when looking from above. Nevertheless, the onset of the fluid-gas coexistence was rather well defined. The acceleration at which the phase transition takes place was determined repeatedly, and did not change by more than 2%. It is possible though, that there is an unknown systematic error, since the gas bubble might nucleate earlier but unnoticed (on top of the fluid phase).

In the second regime, $0.03 \leq W \leq 0.05$, the fluid-gas coexistence was clearly visible. The gas bubble was more or less round and occupied the whole height of the container, i.e., the bottom plate was visible when looking from above. Prior to its nucleation the sample was very "unsettled". Numerous small fluctuations appeared for a short time and wandered around. It literally looked as if the gas phase permeated the fluid phase. If one were to illustrate the onset of the unsettled phase in the phase diagram in fig. 11, it would be represented by a vertical line which parallels the transition line (F)-(C) at slightly lower energies (the difference between the two vertical lines would be $0.5 \leq \Delta E^* \leq 1$).

The third regime can actually be divided into two parts. At first, for $W \geq 0.06$, averaged-sized gas bubbles popped up during the unsettled phase, but they were unstable and vanished again. Was the injected energy high enough, however, the gas bubble was stable and this value was taken as the onset of the fluid-gas coexistence.

If the liquid content was increased further, $W \geq 0.1$, a stable gas bubble was a very scarce event. Instead, the time span between two gas bubbles decreased with an increasing energy. In fact, at a certain energy the time span became zero. Once a gas bubble vanished, another one appeared simultaneously, only at a different position. Even two coexisting gas bubbles (eventually merging into one) were observed. An example of this phenomenon can be seen in fig. 16. In this case, the energy that corresponds to a time span of zero was taken as the energy defining the phase transition. It should be noted that it became increasingly more difficult to determine the onset of a stable fluid-gas coexistence. An instable gas bubble could easily be mistaken for a stable one, just because it existed for a rather long time. In addition, the boundary of the gas bubble looked very ragged and the gas bubble was not as round anymore. It seemed to have a hard time holding its ground against the fluid. Finally, for $W \geq 0.157$, the gas bubble tended to favor the edge of the container and rarely nucleated away from it.

Phase diagram

Let us take one step back and consider the maximum kinetic energy $E_{wall,\,max}$ which a glass bead can obtain by colliding with the bottom of the container. It is rather intuitive that the more liquid is present in the sample, the more energy is dissipated upon a bridge rupture. If a liquid bridge has more volume, it is able to elongate further before breaking, and thus the critical distance D_{crit}, introduced in section 2, is larger. This in turn leads to a higher bridge rupture energy (see eq. 2.5):

$$\Delta E_{cap} = \int_0^{D_{crit}} \mathrm{d}s\, F_{cap}. \tag{4.6}$$

As a consequence, the glass beads need to have a higher energy as well. Otherwise, they simply wouldn't be fast enough to be able to break a liquid bridge. A look at fig. 17 corroborates this argument. Plotted is $E_{wall,\,max}$ at which the system enters the fluid-gas coexistence against the liquid content. As in section 4.2.3, the weighted mean was calculated for each phase diagram. In this case, however, the data points at low accelerations were omitted. Thus, only the vertical part of the transition line was considered. (see section 4.2.2).

The critical kinetic energy of the beads is indeed an increasing function of the liquid content. As can be seen in fig. 17, a function of the form $E(W) = a\sqrt{W}$ fits the data very well. At this point, it is enlightening to recall the expression

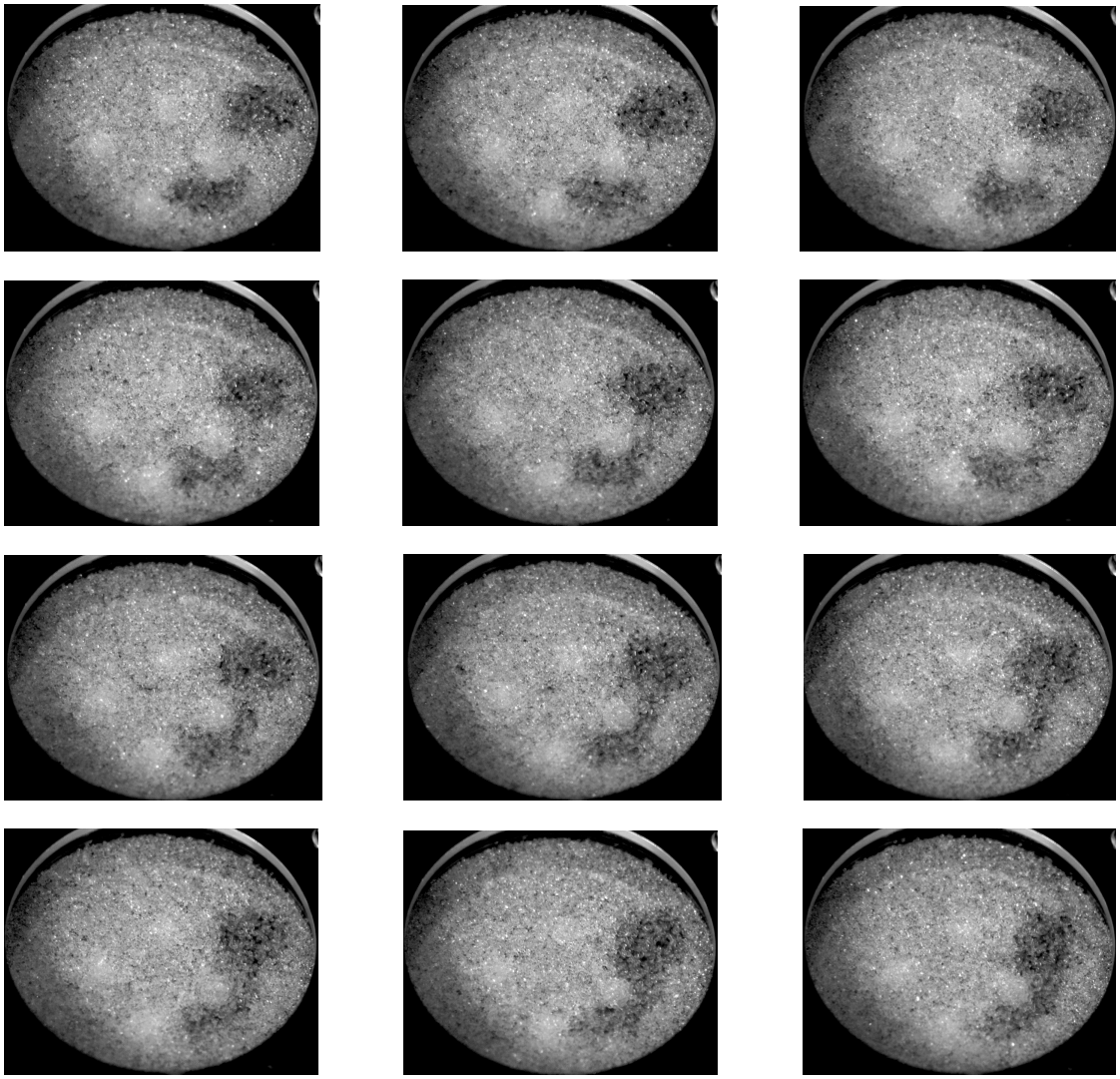

Figure 16: From left to right: Two coexisting gas bubbles merge into a single one. The liquid content is $W = 0.1570 \pm 0.0004$, the frequency $f = 110$ Hz, and the acceleration $\Gamma = 32.0 \pm 1.6$. The time elapsed between the first and the last image is 0.59 s.

of the bridge rupture energy ΔE_{cap} (see eq. 4.5). This quantity scales with $\sqrt{W}$, whereas all other parameters are assumed to be constant. Scaling $E_{wall,\,max}$ with ΔE_{cap} leads to the dimensionless critical energy E_c^* at which the phase transition (F)-(C) occurs. Fig. 18 displays how E_c^* is affected by the variation of the liquid content. Clearly, the critical energy E_c^* is not affected by varying the liquid content over a wide range. The result can be understood in the following way. An increased liquid content increases the bridge rupture energy, as has been pointed out. Fur-

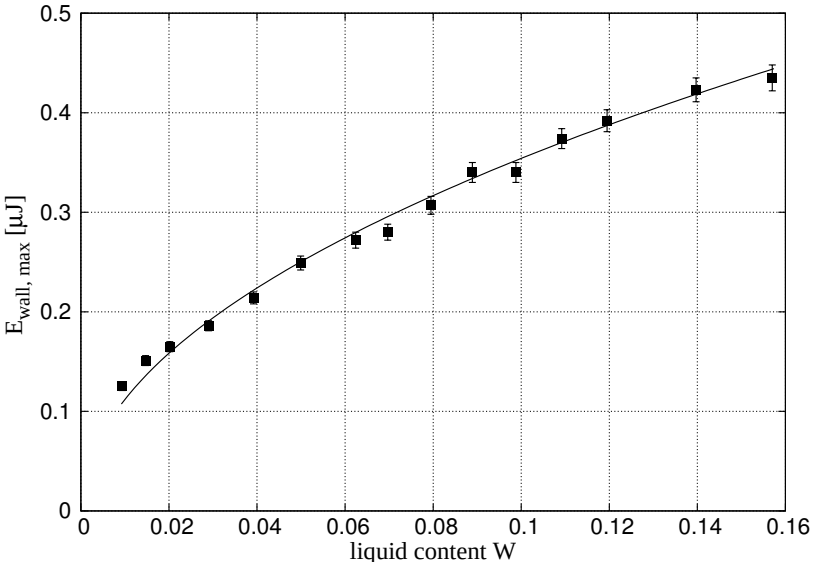

Figure 17: Shown is the dependence of the critical kinetic energy at which the sample enters the fluid-gas coexistence against the liquid content. Each data point represents the weighted mean of one measurement. The solid curve is fitted to the data points and scales as $W^{1/2}$.

thermore, it has been argued that the phase transition (F)-(C) takes place when the energy of the beads (injected into the system by collisions with the container walls) is sufficient to break a liquid bridge. Finally, fig. 18 shows that the required energy for the phase transition is $E_{wall,\,max} = E_c^* \cdot \Delta E_{cap} = \text{const.} \cdot \Delta E_{cap}$. Therefore, the onset of the fluid gas-coexistence does only depend on the bridge rupture energy.

For low liquid contents, $W \leq 0.03$, a slight decrease of E_c^* is visible in fig. 18. Those values correspond to a higher energy which needs to be injected from the container walls in order for the phase transition (F)-(C) to take place. This can be seen in fig. 17, since the first data points lie above the solid line which scales as $\sqrt{W}$. If the bridge rupture energy were the dominating source of energy dissipation determining the nucleation of the gas bubble, $E_{wall,\,max}$ would increase as $\sqrt{W}$.

Two additional effects might come into play for low liquid contents. First, the roughness of the glass beads and the container could become important. If there are crevices present, they are filled by the liquid first and no capillary bridges can develop. Second, fractions of the silicon oil could creep up the container walls and finally out of the container and therefore not interact with the sample. This process would be more noticeable for lower liquid contents. Both scenarios would lead to a

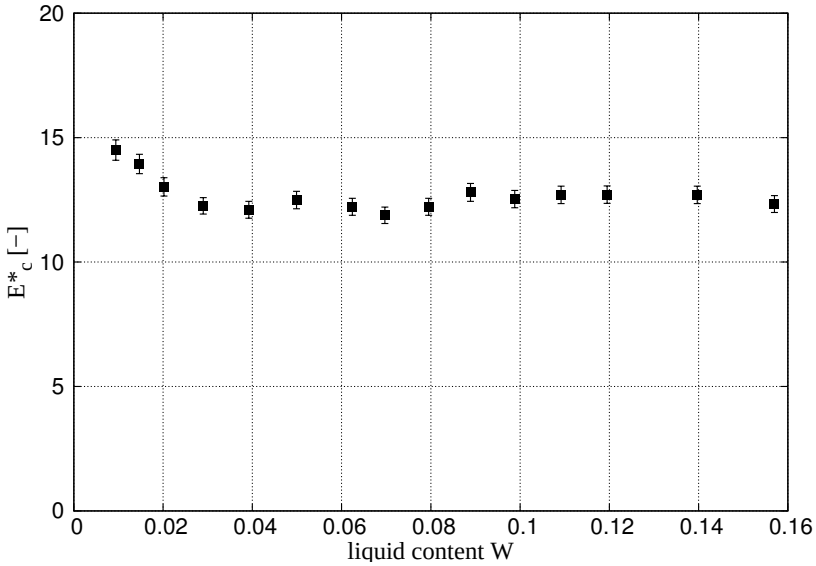

Figure 18: Shown is the dependence of the dimensionless critical energy at which the sample enters the fluid-gas coexistence against the liquid content. Each data point represents the weighted mean of one measurement.

lower effective liquid content, and the bridge rupture energy would be less. This in turn would mean that the glass beads need less energy to break a bridge and the required energy injected by the container walls would be less as well. Clearly, that is not the case. On the contrary, in the experiment, the injected energy is higher, which would correspond to an increased effective liquid content.

As was stated in the above paragraph "Visual changes", the gas bubble was hard to make out for low liquid contents and a systematic error might have influenced the measurement of the onset of the gas bubble. Eventually, the gas bubble nucleated at lower energies, but it was on top of the fluid phase, and unnoticed. This might account for the seemingly higher required energy $E_{wall,\,max}$ in fig. 17. Especially the fact that the regime in which the gas bubble was clearly visible begins at $W = 0.03$ points to a possible connection between the weak gas bubble and the higher required energies. In order to rule out random errors, the measurements for low liquid contents were repeated. The results are reproducible with a deviation of 2%[3].

Considering fig. 18, two separate linear regressions for $W < 0.03$ and $W \geq 0.03$ were performed. It turns out that the two linear fits intersect at $W = 0.026 \pm 0.004$. A figure showing the linear regressions as well as their intersection can be found in

[3]Repetitions of a few measurements with randomly chosen liquid contents were performed as well. Those also show a high reproducibility.

Appendix E (fig. 31). In section 2.2 it was shown that only in the liquid content regime $10^{-3} \lesssim W \lesssim 0.024$ single capillary bridges exist. Apparently, the upper boundary coincides with the intersection of the two linear regressions. Therefore, increasing the amount of liquid while the sample is in the single capillary bridge regime causes an additional change of the phase transition (F)-(C) which is not due to the bridge rupture energy. For low liquid contents, the transition line in the phase diagram is still a vertical one (see Appendix D, fig. 26), i.e., the phase transition is also solely energy dependent. This indicates that other sources of energy dissipation might play a role in this liquid content regime. Nevertheless, the bridge rupture energy is dominating, since the additional energy dissipation mechanisms cause only a small change of the critical energy E_c^* when the liquid content is varied. Comparing the value of E_c^* at $W = 0.0094$ with the one at $W = 0.0029$ in fig.18 shows that they deviate by 17%. Once the critical liquid content at which the single liquid bridges coalesce is reached, E_c^* is independent of W and the phase transition is solely determined by the bridge rupture energy.

To conclude, the bridge rupture energy serves as a formidable scaling factor for the energy. The onset of the fluid-gas coexistence occurs at a constant critical energy E_c^* over a wide range of liquid contents. This is even more fascinating, when considering that the bridge rupture energy is merely a notional quantity for $W \gtrsim 0.024$. Although no single liquid bridges are present, the phase transition (F)-(C) can be described by the rupture of such bridges.

4.2.5. Effect of a varying liquid content on the phase transition (C)-(G)

Let us now turn to the phase transition (C)-(G) at which the sample enters the gaseous phase. As was pointed out in section 4.2.2, the phase transition (C)-(G) is represented by a line in the phase diagram which rises first and then becomes vertical. In contrast to the phase transition (F)-(C), the position of this transition line depends to a larger degree on the liquid content. The gradual change of the phase transition can be seen in fig. 19. Displayed are several transition lines in a phase diagram, whereas the lines have been obtained at different liquid contents. Apparently, for higher liquid contents, the transition line experiences a shift toward lower energies. At a certain liquid content, however, the position of the transition line does not seem to change anymore. In order to quantify this observation, a similar approach as in the two previous sections was taken. For each transition line,

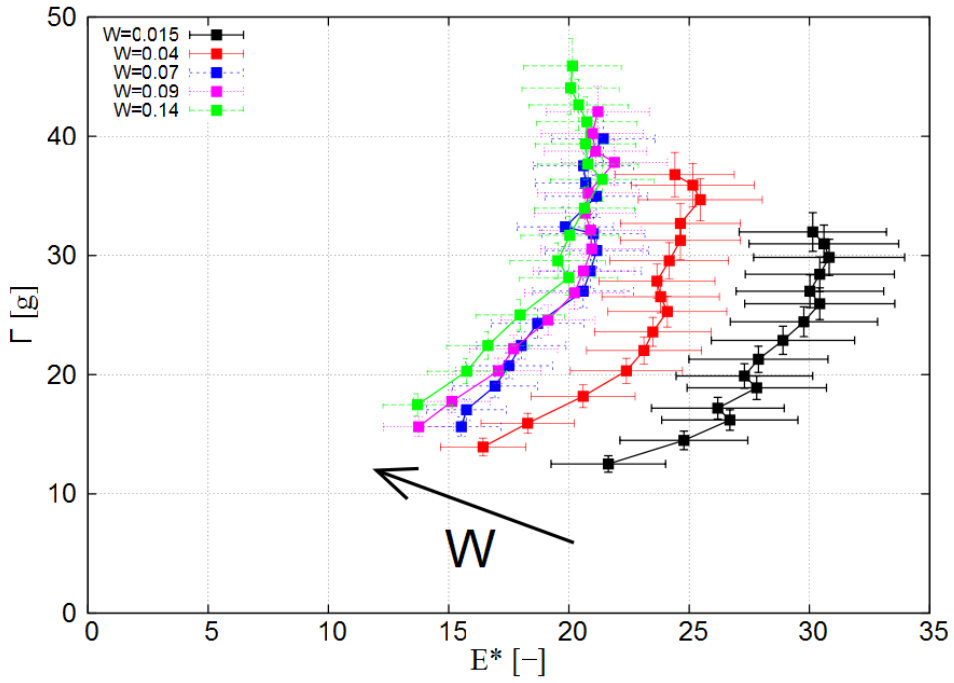

Figure 19: Phase transition (C)-(G) in a phase diagram. The arrow depicts the direction of an increasing liquid content W.

only the vertical part where the critical energy E_g^* is constant was considered. In this section, the critical energy E_g^* denotes the phase transition from the fluid-gas coexistence to the gaseous phase. Taking the data points of the vertical line into account, a weighted mean was calculated for each phase diagram and plotted against the liquid content. The result can be seen in fig. 20.

The curve decreases at first, although the measurement at $W = 0.029$ seems to differ from the other ones. It is an interesting finding, that for $W \gtrsim 0.07$ the curve does not decrease any further, but rather stays constant. Scheel et al. [16] suggested, that a percolation transition takes place around $W = 0.08$ [4]. Therefore, the change of E_g^* in fig. 20 around $W = 0.07$ might be attributed to the onset of percolation.

As is the case with the phase transition (F)-(C), the energy which is required for the phase transition (C)-(G) is an increasing function of the liquid content. The more liquid is added, the more energy the system needs to enter the gaseous

[4] A look at fig. 4 corroborates their argumentation, because the volume of the largest cluster increases drastically around that liquid content.

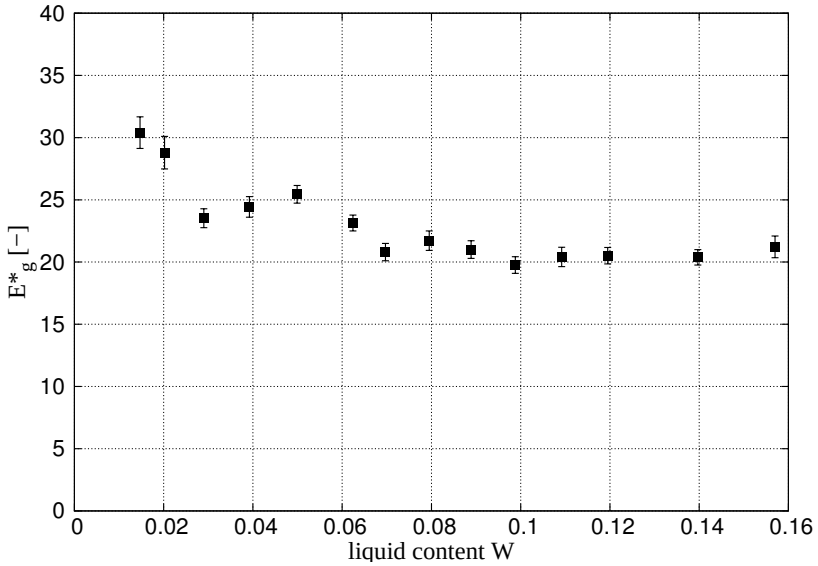

Figure 20: Shown is the dependence of the dimensionless critical energy, at which the sample enters the gaseous phase, against the liquid content. Each data point represents the weighted mean of the vertical part of the transition line.

phase. This relation is shown in Appendix E (fig. 32). Let us recall how the gas phase is defined: The glass beads occupy the whole container (from bottom to top), and the energy of the beads must be sufficient to break a liquid bridge after every collision and to be lifted up. As in the previous section, the scaling of the energy with the bridge rupture energy is appropriate for larger liquid contents. Prior to that, the glass beads seem to require more energy in order to move around freely in the container. This time, however, the critical energy in fig. 20 at $W = 0.0147$ deviates by 50% from the value at $W = 0.0697$. Clearly, the onset of the gaseous phase depends on more than just the bridge rupture energy for lower liquid contents. Again, different energy dissipation mechanisms due, for example, to frictional forces or viscosity, might play a role in the lower liquid content regime. The viscous force is proportional to the relative velocity of the particles and the latter is about one third larger at the phase transition (C)-(G) than at the phase transition (F)-(C). Therefore, the viscous force could have a greater effect.

During the measurements, the gas phase was entered once no fluid phase was visible anymore. In each measurement, the gas bubble pushed away the fluid phase until at last, the fluid phase was only present within a narrow band, having a thickness of approximately three bead diameters, along the container wall. In order

to let this last part of the fluid phase vanish, a relatively large increase of the acceleration was necessary (compared to the growth of the gas bubble up to this point). Thus, it might be possible that the interaction of the glass beads with the container wall prolongs the fluid-gas coexistence. This indicates that the geometry of the experimental setup influences the phase transition (C)-(G) as well.

Whatever causes the required energy in the lower liquid content regime to be higher, its influence becomes negligible compared to the rupture of a liquid cluster for $W \gtrsim 0.07$.

4.2.6. Effect of a varying liquid content on the phase diagram

So far, we have taken a look at each phase transition individually. Let us now consider how the whole phase diagram is affected by varying the liquid content. The phase transition (S)-(F) is not affected at all and will be ignored in the following. However, the shape of the fluid-gas coexistence does change with the liquid content. The changing boundaries of the coexistence region are displayed in fig. 21.

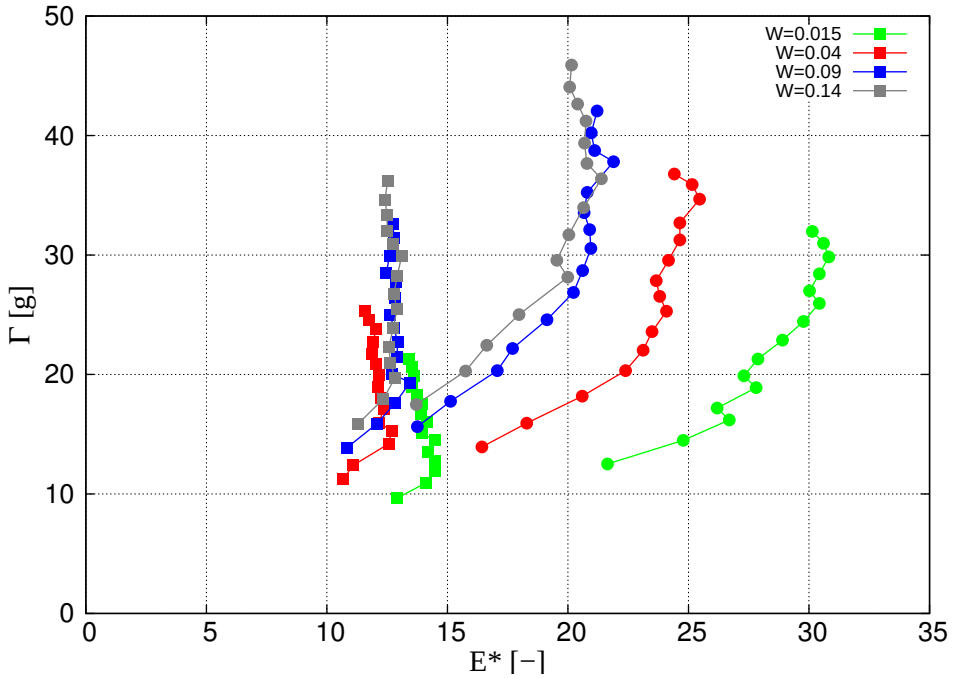

Figure 21: Shown is the phase diagram obtained at different liquid contents. The data points represent the phase transition (F)-(C) (squares) and the phase transition (C)-(G) (circles). For the sake of clarity error bars are omitted. The lines are merely connecting the data points and indicate the boundaries of the fluid-gas coexistence.

First of all, the phase transition (F)-(C) is represented by a more or less vertical line (if one ignores the first two data points). Clearly, scaling the energy with the bridge rupture energy causes the individual phase transition lines to collapse on a single vertical line. Therefore, while adding more liquid to the sample causes drastic changes in the liquid morphology, the phase transition can nevertheless be described by the rupture of single bridges and the corresponding dissipation of energy.
Second, as it was pointed out in section 4.2.5, the phase transition (C)-(G) experiences a shift toward lower energies with an increasing liquid content. At a liquid content $W \approx 0.07$, a further shift cannot be observed anymore and the position of the transition line is unchanged.

Hence, at first, the coexistence region diminishes with an increasing amount of liquid, whereas the qualitative shape of the boundaries stays the same. In other words, the energy band $E_c^* \leq E^* \leq E_g^*$ in which a fluid-gas coexistence can be observed decreases. For $W \gtrsim 0.07$, however, the onset and the disappearance of the fluid-gas coexistence seems to be solely dependent on the rupture of liquid clusters, whereas the latter depends on the liquid content as $\Delta E_{cap} \propto \sqrt{W}$

At this point, one might wonder why the vertical transition lines shift upwards with an increasing liquid content, although the corresponding phase transitions are supposedly independent of the force. The answer becomes clear when the experimental setup is considered again. On the one hand, it has been shown that the glass beads need to have a certain critical energy in order for a phase transition to take place. On the other hand, this critical energy increases with increasing the liquid content (see fig. 17 and 32). In the setup used in this thesis, energy is only injected into the system by collisions of the glass beads with the container walls. Therefore, in order to inject more energy, the container walls need to move faster. The maximum velocity of the container walls is $v = a \,/\, 2\pi f$, where a is the maximum acceleration of the container. Since the same frequency range, namely $60\,\mathrm{Hz} \leq f \leq 130\,\mathrm{Hz}$, was considered in each measurement, only a larger acceleration can cause an increase in the velocity of the container. Thus, the energy dependent transition lines in the phase diagram occur at higher dimensionless accelerations $\Gamma = a \,/\, g$.

5. Summary

In wet granular matter, small capillary bridges form at the contact areas of neighboring beads and exert an attractive force on the beads. Thus, the material is much stiffer than its dry counterpart. Adding more and more liquid to the sample causes the growing of the capillary bridges, i.e., the volume of such a bridge is increased. At a certain liquid content threshold, the bridges start to coalesce and the morphology of the liquid structures changes drastically.

In this thesis it was investigated whether an increase of the liquid content affects the dynamical phase transitions of wet granular matter. The phase transitions were due to the dissipation of energy when a liquid bridge ruptures. Depending on the balance between injected and dissipated energy, the system resided in either a solid, fluid or gaseous phase. A fluid-gas coexistence existed as well, whereas it expressed itself as a gas bubble which was less dense than the surrounding fluid phase. A phase diagram was constructed in order to facilitate the analysis of the different phase transitions.

The experimental setup consisted of a shaker which applied a vertical agitation to a pile of glass beads mixed with a well defined amount of a wetting liquid in a flat container. By varying the frequency and amplitude of the vibration, the two parameters characterizing the phase diagram, i.e., the maximum energy and acceleration of the container bottom, could be adjusted independently. Early on, it was found that water was not a suitable choice in this experiment. Water is known for interacting with the surface of glass. At high accelerations, this reaction eventually led to a failure of the glass beads when colliding with the container wall or each other. As a consequence, very small glass particles could be observed in the sample, drastically changing the characteristics of the sample in an unpredictable manner.

Another liquid with wetting properties on glass is silicon oil, which was then used throughout the experiments. Phase diagrams were constructed at different liquid contents ($0.0094 \leq W \leq 0.157$) and compared with each other. First, it was found that the phase transition from solid to fluid is independent of the energy injected by the container walls as well as the liquid content. Both findings are in agreement with earlier experiments [11, 15]. Thus, this phase transition is solely determined by the capillary force which is exerted on the glass beads by the liquid in the sample. In addition, the capillary force does not seem to change when more liquid is present in the sample, causing single liquid bridges to coalesce to form larger liquid clusters.

Next, the onset of the fluid-gas coexistence was explored. The corresponding phase transition was found to be largely independent of the acceleration of the container, and thus of the force acting on the beads. Instead, as Huang et al. [11] argued, the phase transition takes place when the kinetic energy of the glass beads is sufficient to break a liquid bridge. Comparing the phase diagrams obtained at different liquid contents with each other revealed that the bridge rupture energy is a good scaling factor of the energy in the system. At higher liquid contents, the phase transition can still be described by the bridge rupture energy, although single liquid bridges are no longer present in the sample. Therefore, the changes of the liquid morphology due to higher liquid contents do not affect the dynamical phase transition from the fluid phase to fluid-gas coexistence. Furthermore, an additional energy dissipation mechanism might play a minor role in the liquid content regime in which single capillary bridges exist.

A third phase transition led from the fluid-gas coexistence to the gaseous phase. This phase transition is neither represented by a horizontal nor a purely vertical line in the phase diagram. The shape of the transition line is in good agreement with earlier simulations concerning wet granular matter under vertical agitation [14]. It was found that up to the liquid content $W = 0.07$, the position of the transition line in the phase diagram depends to a great extent on the liquid content. Apparently, the phase transition is influenced by the coalescing process of the liquid bridges, in contrast to the previous two. For liquid contents higher than $W = 0.07$, the bridge rupture energy is again a good energy scale. Interestingly, it was observed in the past that a percolation transition takes place in wet granular matter around that liquid content [15]. Certainly, the complexity of this third phase transition encourages further studies. In addition, it would be worthwhile to address the influence of the liquid's viscosity on the dynamical phase transitions.

Appendix

A. Cleaning protocols

The cleaning procedures were applied before each measurement, in order to guarantee reproducible starting conditions.

A.1. Glass beads

One set of glass beads for one measurement was cleaned individually. One portion of MÜHLMEIER Mahltechnik glass beads had the mass of about $m_{beads} = 125$ g (corresponding to a volume of $V_{beads} = 78$ ml) and was put into a beaker with a volume of $V = 1$ L. Next the following steps were performed:

1. Tapped water was filled into the beaker until the glass beads were covered. A gentle shaking of the beaker was applied for a couple of minutes. Afterwards the water was slowly poured out of the beaker without loosing any beads.
2. Ethanol was poured into the beaker and step 1 was repeated. After having drained the ethanol, distilled water was applied several times to dilute the ethanol.
3. Step 2 was repeated with Acetone.
4. The wet glass beads in the beaker were dried in a oven at the temperature 120° over night.
5. Before using the glass beads they cooled of for at least three hours. It was confirmed by touch that they indeed had cooled down to room temperature.

Cleaning one set at time had the advantage that only the bottom part of the beaker was filled with glass beads. Therefore, the applied shaking was swirling around every bead. Earlier attempts with more glass beads showed that only the beads on top were influenced by the shaking. The beads at the bottom did not move at all.

A.2. Container

The container consists of two glass petri dishes: one serving as the bottom and the other one as the lid (see Appendix C). The following steps were performed on each dish before every measurement:

1. The glass was roughly cleaned with a tissue paper soaked with tapped water, and dried afterwards (with a tissue paper as well).

2. Step 1 was repeated with Ethanol and Acetone and distilled water.

3. The glass was completely dried with tissue paper.

After a measurement, the container was covered with silicone oil, which does not solve in water. Therefore, the following steps were performed after each measurement, in order to get completely rid of the silicon oil:

1. The glass was repeatedly wiped of with a tissue paper soaked with Acetone.

2. Next, Isopropanol was applied and washed of with distilled water.

3. Repetition of steps 1 and 2 were repeated until no traces of silicon oil were visible anymore.

B. Determining the density of silicon oil

The silicon oil (ELBESIL-ÖL B5) was obtained "L. Böwing GmbH". The density ρ_{oil} was determined experimentally in the following way:

1. An empty container (15ml) with a 0.5ml scale division was weighted on a precision balance.

2. A small amount of silicon oil was poured into the container, and its volume was determined.

3. The mass of the container with the liquid was measured on a precision balance.

4. Repetition of steps 2 and 3 for the same container (the liquid was added to the amount that was already in the container).

Steps 1-4 were conducted three times. For each measurement with one container, the mass of silicon oil (after having subtracted the container weight) was plotted against its volume. A linear regression was performed and the slope α_i with the corresponding error σ_{α_i} was determined with GNUPLOT. The results of the three measurements are displayed in fig. 22. Both error bars (horizontal and vertical) were taken into account, but the vertical error of the mass is to small to be seen

in the graph. The error bars equal the last digit of the precision scale ($\sigma_m = 0.01$ g) and half of the scaling division of the container ($\sigma_V = 0.25$ ml) of the mass and volume, respectively.

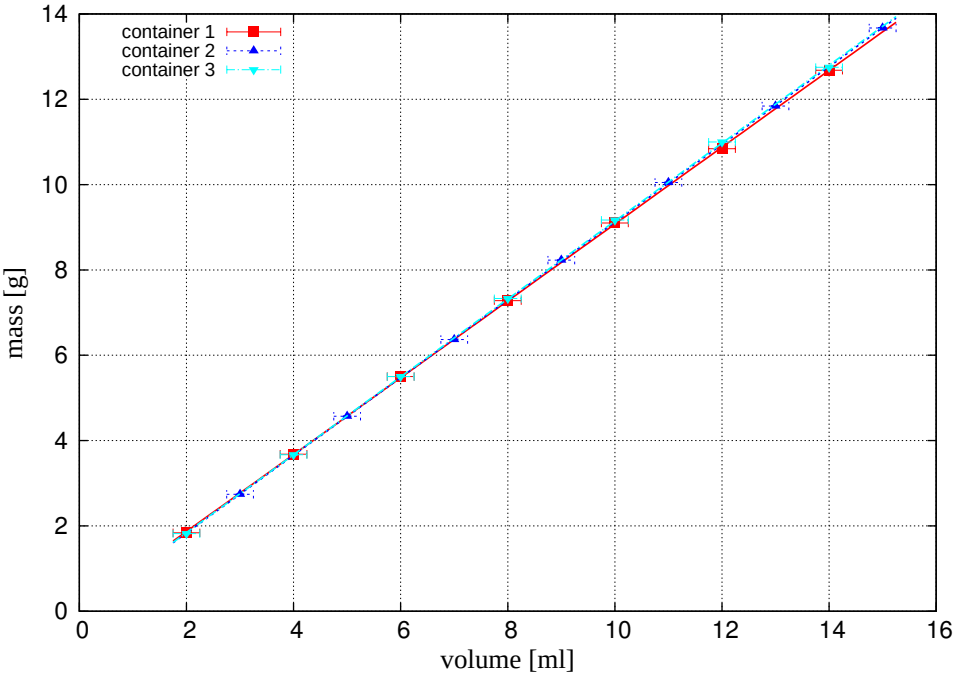

Figure 22: Linear regressions of three measurements determining the density of silicon oil

Next, the weighted mean $\overline{\alpha}$ was calculated. This value is taken as the density ρ_{oil} in this thesis:

$$\rho_{oil} = \overline{\alpha} = (913 \pm 2)\,\frac{\mathrm{Kg}}{\mathrm{m}^3}. \tag{B.1}$$

C. Pictures of the setup

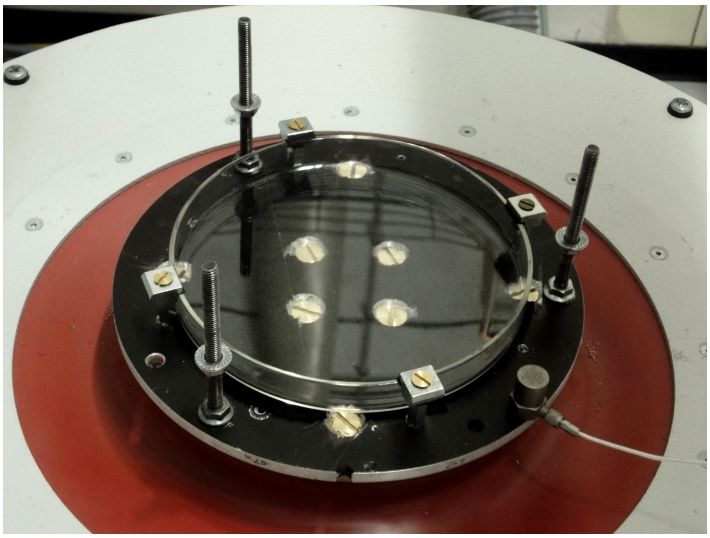

Figure 23: Bottom part of the setup: shown is the petri dish, which is secured with four clamps. The accelerometer is bolted directly to the bottom plate.

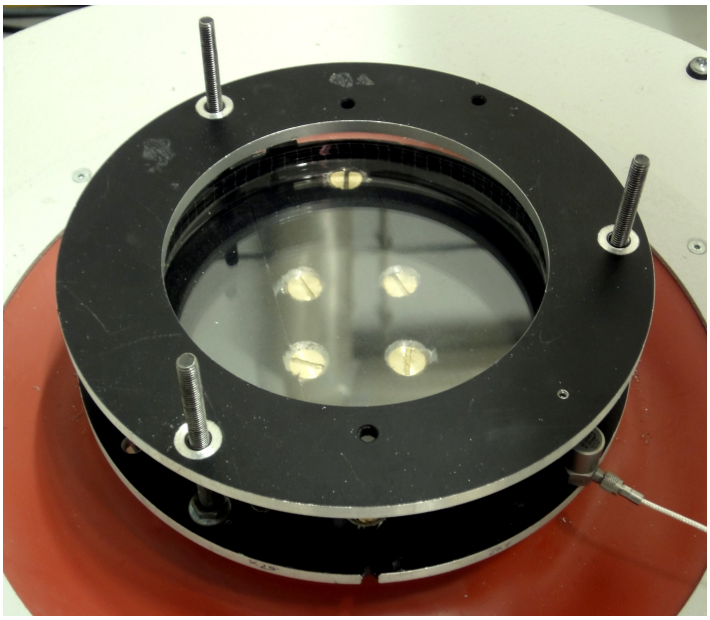

Figure 24: Upper part of the setup: shown is the lid, consisting of a petri dish glued to the upper plate. The petri dish is slightly smaller than the bottom one. That way, it can slide into the bottom petri dish and completely seal the container. Furthermore, the height of the container can be adjusted by moving the lid up and down.

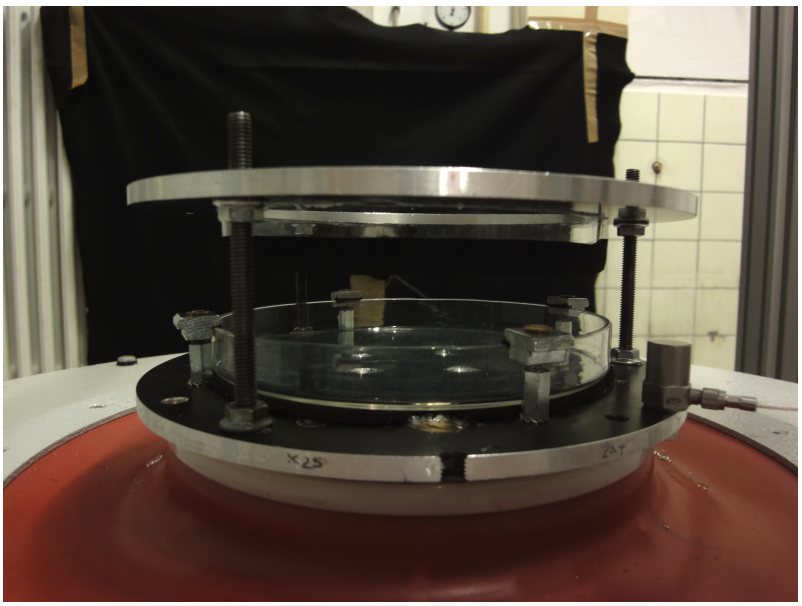

Figure 25: Side view of the setup.

D. Phase diagrams

Displayed are phase diagrams of glass beads wetted with silicon oil at different liquid contents W, spanned by the externally applied frequency and the peak acceleration. Each square represents the measured data pair (f, Γ) when a phase transition takes place. The colored regions correspond to the different phases of the system: solid (red), fluid (green), fluid-gas coexistence (white) and gas (yellow). The unexplored region is depicted by black dots.

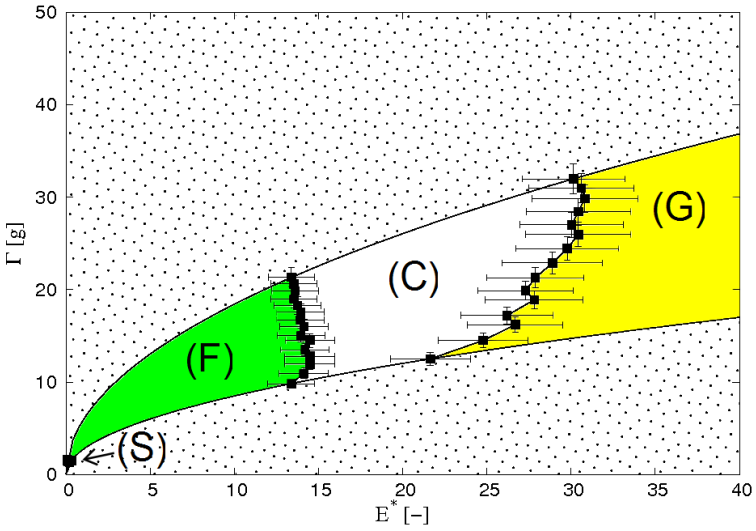

Figure 26: $W = 0.0147 \pm 0.0002$

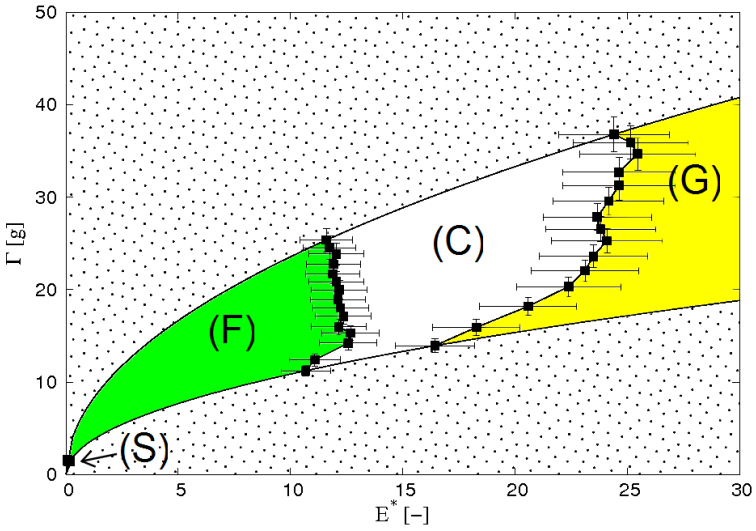

Figure 27: $W = 0.0392 \pm 0.0002$

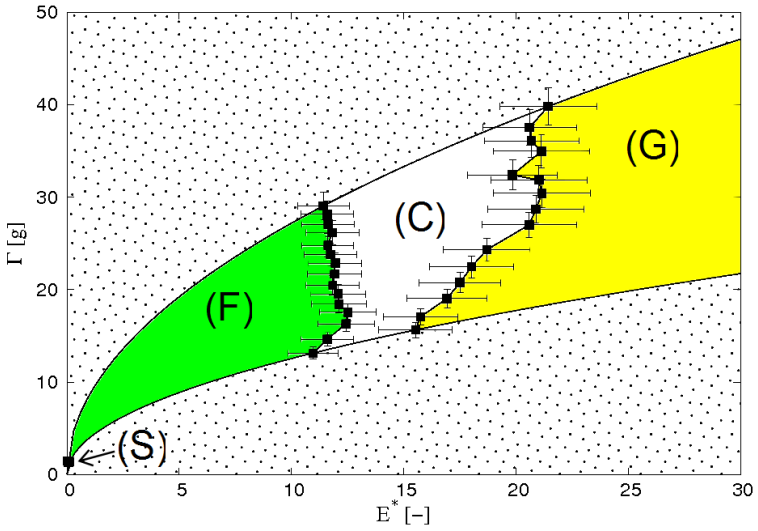

Figure 28: $W = 0.0697 \pm 0.0002$

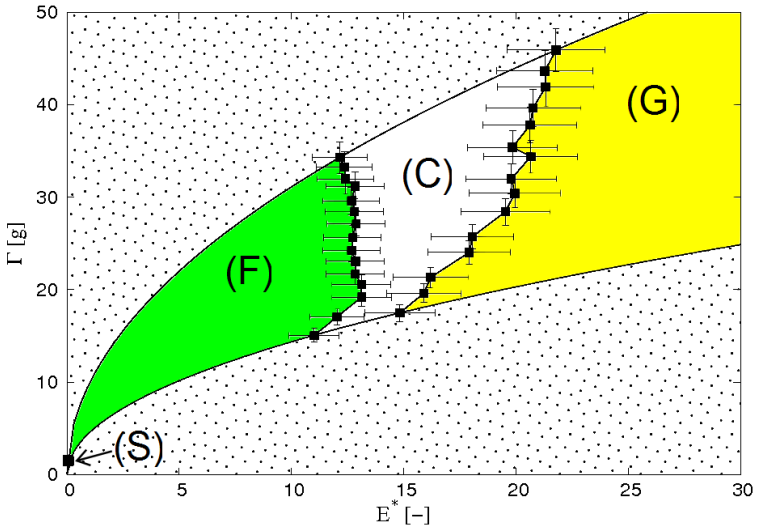

Figure 29: $W = 0.1195 \pm 0.0003$

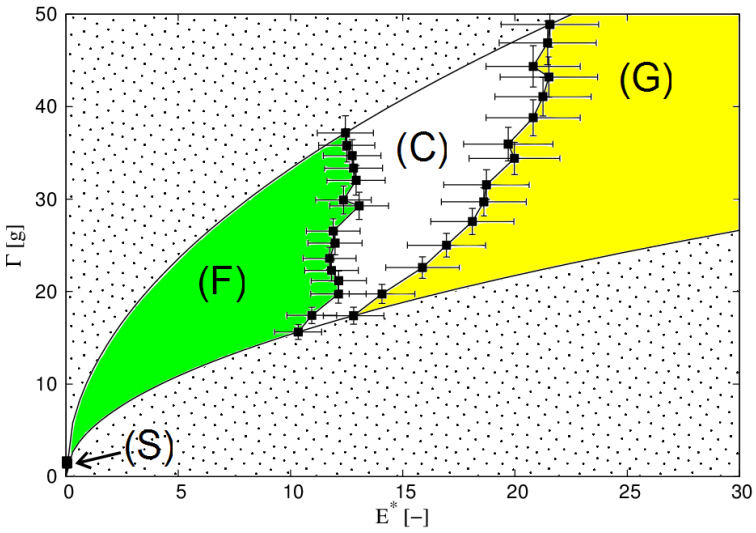

Figure 30: $W = 0.1570 \pm 0.0004$

E. Additional Figures

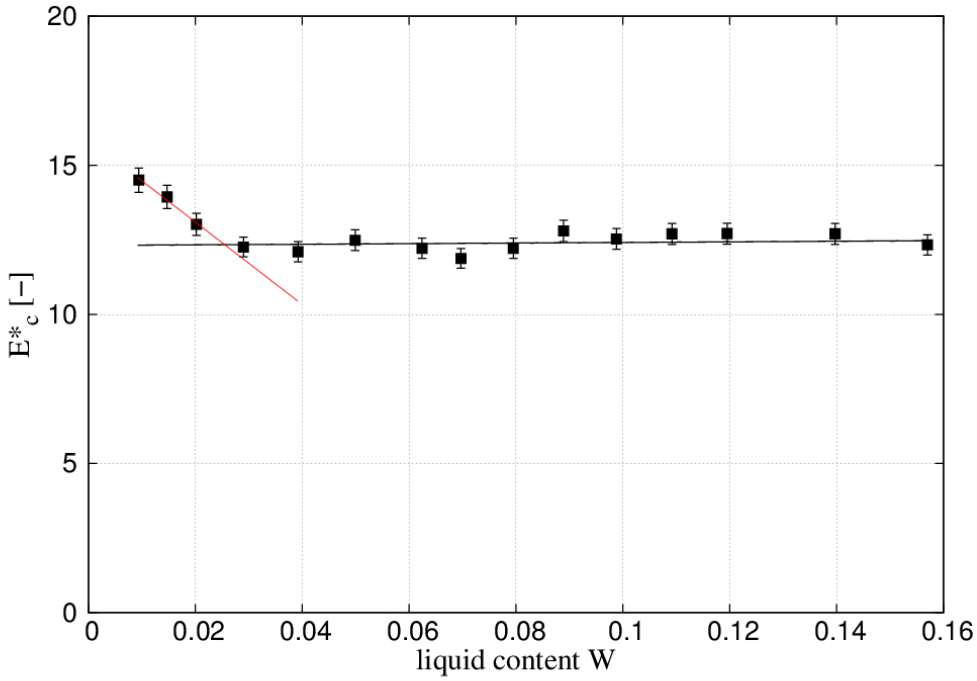

Figure 31: Shown are the same data points as in fig.17. The two solid lines represent linear regressions and their intersection denotes the onset of the horizontal part.

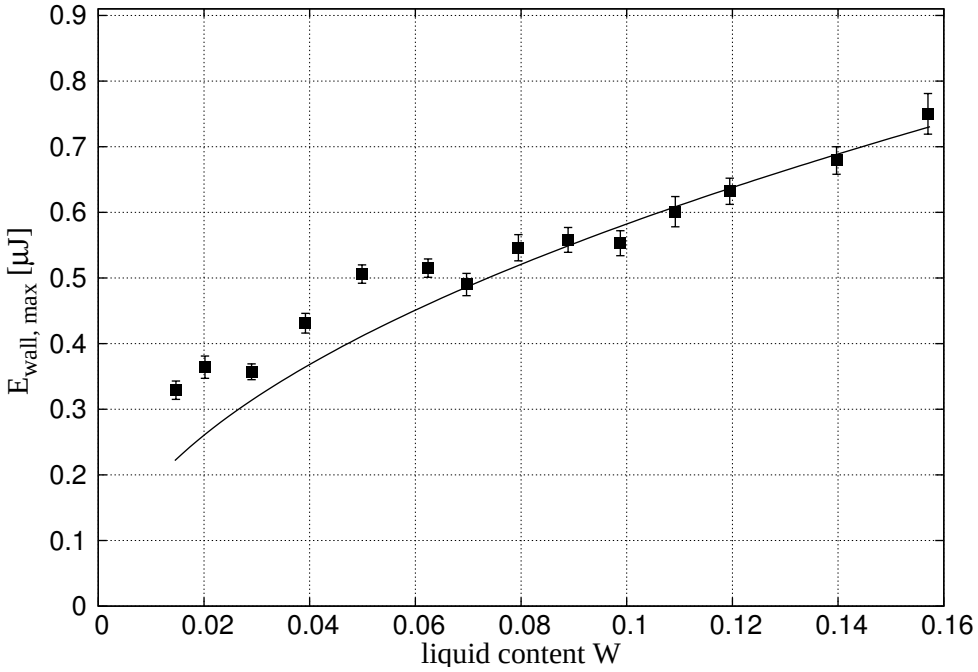

Figure 32: Shown is the dependence of the critical kinetic energy at which the sample enters the gaseous phase against the liquid content. Each data point represents the weighted mean of the vertical part of the transition line. The solid curve is fitted to the data points and scales as $W^{1/2}$.

Acknowledgements

First of all, I would like to thank my supervisor Prof. Dr. Stephan Herminghaus for his support throughout my research. Especially his helpful advices and encouragement enabled me to finish this thesis. I would also like to thank the reviewer of this thesis, Prof. Dr. Annette Zippelius.

Furthermore, I would like to thank Dr. Kai Huang for introducing me to the experimental setup which was used in this research. At all times, he was willing to answer my questions and share his thoughts. My sincere thanks to Wolf Keiderling who helped me to modify the experimental setup in order to meet my requirements. I would like to thank Chih-Wei Peng for showing me how to use the camera and other crucial parts of the measurement system.

Very special thanks to Andreas Hüper with whom I had numerous eye-opening discussions. I would also like to thank Klaus Röller for discussing his simulations and results with me. In addition, I thank Dr. Ruth Klauser who donated her time to proofread this thesis. Finally, I would like to thank my family for supporting and encouraging me throughout this period.

References

[1] The propagation of uncertainty of the error of the quantity A as a function of the quantities $B_{1,\ldots,n}$ is calculated in the following way: $\sigma_A = \sqrt{\sum_{k=1}^{n} \left(\frac{\partial A}{\partial B_k} \cdot \sigma_{B_k} \right)^2}$

[2] Antonyuk, Sergiy ; Heinrich, Stefan ; Palzer, Stefan: Impact behaviour of particles with liquid films: energy dissipation and sticking criteria. In: *2010 ECI Conference on The 13th International Conference on Fluidization - New Paradigm in Fluidization Engineering*, 2011

[3] Bernal, J.D. ; Mason, J.: Packing of Spheres: Co-ordination of Randomly Packed Spheres. In: *Nature* 188 (1960)

[4] Bunker, B.C.: Molecular mechanisms for corrosion of silica and silicate glasses. In: *Journal of Non-Crystalline Solids* 179 (1994)

[5] Butt, Hans-Jürgen ; Kappl, Michael: Normal capillary forces. In: *Advances in Colloid and Interface Science* 146 (2009)

[6] Dalgiesh, W.Alan: Design of glass and glazing for wind pressure and rain. In: *Wind effects on buildings and structures.* J.D. Riera & A.G. Davenport Editors), 1998, S. 243–262

[7] Duran, Jaques: *Sands, Powders and Grains: An Introduction to the Physics of Granular Materials.* Springer-Verlag New York, Inc., 2000

[8] Fingerle, Axel ; Röller, Klaus ; Huang, Kai ; Herminghaus, Stephan: Phase transistions far from equilibrium in wet granular matter. In: *New Journal of Physics* 10 (2008)

[9] GmbH, L. B.: *Technische Information, ELBESIL-ÖLE.* – The data sheet was sent to me on request

[10] Herminghaus, Stephan: Dynamics of wet granular matter. In: *Advances in Physics* 54 (2005)

[11] Huang, Kai ; Röller, Klaus ; Herminghaus, Stephan: Universal and non-universal aspects of wet granular matter under vertical vibrations. In: *The European Physical Journal Special Topics* 179 (2009)

[12] KISTLER: *K-Shear Beschleunigungssensoren, Typ 8702B..., 8704B...* 2008. – The data sheet can be downloaded from http://www.kistler.com

[13] MÜHLMEIER MAHLTECHNIK: *Produktinformation - MINI-BEADS, bleifrei.* 2008. – The data sheet was sent to me on request

[14] RÖLLER, Klaus: *Numerical simulations of wet granular matter*, Georg-August-Universität Göttingen, Dissertation, 2010

[15] SCHEEL, M. ; SEEMANN, R. ; BRINKMANN, M. ; MICHIEL, M. D. ; SHEPPARD, A. ; BREIDENBACH, B. ; HERMINGHAUS, S.: Morphological clues to wet granular pile stability. In: *nature materials* 7 (2008)

[16] SCHEEL, M. ; SEEMANN, R. ; BRINKMANN, M. ; MICHIEL, M. D. ; SHEPPARD, A. ; HERMINGHAUS, S.: Liquid distribution and cohesion in wet granular assemblies beyond the capillary bridge regime. In: *Journal of Physics: Condensed Matter* 20 (2008)

[17] SCHEEL, Mario ; GEROMICHALOS, Dimitrios ; HERMINGHAUS, Stephan: Wet granular matter under vertical agitation. In: *Journal of Physics: Condensed Matter*

[18] STÖCKER, Prof. Dr. H.: *Taschenbuch der Physik.* Verlag Harri Deutsch, 2004

[19] WILLETT, Christopher D. ; ADAMS, Michael J. ; JOHNSON, Simon A. ; SEVILLE, Jonathan P.: Capillary Bridges between Two Spherical Bodies. In: *Langmuir* 16 (2000)

Erklärung nach §13(8) der Prüfungsordnung für den Bachelor-Studiengang Physik und den Master-Studiengang Physik an der Universität Göttingen:

Hiermit erkläre ich, dass ich diese Abschlussarbeit selbständig verfasst habe, keine anderen als die angegebenen Quellen und Hilfsmittel benutzt habe und alle Stellen, die wörtlich oder sinngemäß aus veröffentlichten Schriften entnommen wurden, als solche kenntlich gemacht habe.
Darüberhinaus erkläre ich, dass diese Abschlussarbeit nicht, auch nicht auszugsweise, im Rahmen einer nichtbestandenen Prüfung an dieser oder einer anderen Hochschule eingereicht wurde.

Göttingen, den 21. März 2011

(Stefanie Strauch)